UNIVERSITY OF TWENTE

The effect of Arctic precipitation changes on the Atlantic meridional overturning circulation

Master thesis

Niek van der Sleen
October 11, 2015

UNIVERSITEIT TWENTE.

Koninklijk Nederlands
Meteorologisch Instituut
Ministerie van Infrastructuur en Milieu

The effect of Arctic precipitation changes on the Atlantic meridional overturning circulation

Date	October 11, 2015	
Version	Final version	
Author	Niek R. van der Sleen	
Contact	niekvandersleen@gmail.com	
University	University of Twente	
Faculty	Engineering Technology (CTW)	
Program	Water Engineering and Management	
Graduation committee	Prof. dr. S.J.M.H. Hulscher (chair)	University of Twente
	Dr. K. Wijnberg (daily supervisor)	University of Twente
	Dr. R. Bintanja (daily supervisor)	KNMI
	Dr. C.A. Katsman	Delft University of Technology

Abstract

In this study the effect of an increase in precipitation on the Atlantic meridional overturning circulation (AMOC) is studied. The processes involved that lead to a weakening of the AMOC, like the change in sea surface salinity, mixed layer depth and sinking are described and explained. This research is done because the IPCC expects an increase in precipitation of more than 50 % in some parts of the Arctic region with the RCP 8.5 scenario. The expected result of an increase in precipitation is that a relatively fresh surface layer will form on the ocean. If this is the case in the convection regions, the fresh surface layer will prevent convection to occur and therefore indirectly affect the AMOC.

This study continues on the research performed by Bintanja & Selten (2014). They have performed model runs in which the precipitation above the Arctic Ocean is changed. The change in precipitation in the model runs range from a -50 % decrease to a +300 % increase of precipitation above the Arctic Ocean north of 70 °N. The model runs are performed with the coupled atmosphere (IFS), ocean (NEMO) and sea ice model (LIM) EC-Earth. The used version is 2.3 with a 1 degree resolution. Besides the model runs performed by Bintanja & Selten also new model runs are performed to further study the effect of an increase in precipitation above 80 degrees north.

The mixed layer depths and the AMOC are more sensitive to an increase in precipitation above the Arctic Ocean compared to the sea surface salinities. This is because the sea surface salinities have a much smaller natural variability. The sea surface salinities decrease with 6.8 %, the maximum mixed layer depth with 76 % and the strength of the AMOC decreases 43 % in the model run in which the precipitation is increased with 400 % in the region above 70 degrees north.

Density profiles near the convection regions show that there will indeed form a layer of relatively fresh surface water on top of the ocean. This makes that the convection in these regions is much less. For the Nordic Seas this means that the deeper layers will be less dense, which results in less overflow at the Greenland Scotland ridge. In the Labrador Sea the fresh layer results in small mixed layer depths. This affects the amount of sinking according to the theory of Spall & Pickart (2001) which says that the amount of net sinking is dependent of the mixed layer depth.

It turns out that 10.93 Sv sinks in the North Atlantic Ocean, this makes up a large part of the AMOC which has a strength of 12.91 Sv in the control run. The most important sinking regions in this study are the region west of Great Britain and the overflows at the Greenland Scotland ridge. The sinking region west of Great Britain is not in line with observations, this is an important result and in the further development of EC-Earth it is important to find out what causes the sinking in this region in the model. If the precipitation increases, the sinking as a result of the overflow at the GS ridge and the sinking west of Great Britain are decreasing the most. Therefore most of the decrease in AMOC strength because of an increase in precipitation in the Arctic can be contributed to these regions.

If the precipitation is only increased in the region above 80 degrees north instead of 70 degrees north, the system responds differently. The average value of the mixed layer depth in the Nordic Seas is less affected, also the sinking in the North Atlantic Ocean decrease less. The cause of this is that the precipitation is not directly increased above the convection region in the North Atlantic Ocean. For the strength of the AMOC it does not matter whether the precipitation is increased above 70 degrees north of 80 degrees north.

Acknowledgments

This is the master thesis for my master Civil Engineering and Management with the track Water Engineering and Management. I have done this research in half a year at the Royal Netherlands Meteorological Institute (KNMI). Doing this research at the KNMI was quite a challenge as the subject is a bit outside of the field of Civil Engineering. Because of this I have learned a lot in the past half year.

Of course I couldn't learn so much all by myself, therefore I would like to thank my supervisors Richard Bintanja and Caroline Katsman for creating the opportunity for me to write my master thesis at the KNMI and for their help and feedback during my internship. I would also like to thank my supervisors from the university Suzanne Hulscher and Kathelijne Wijnberg for their critical feedback.

I would also like to thank my friends and family for their support during the whole period of writing my master thesis. Finally I would like to thank my parents for giving me the opportunity to do a bachelor and master study at the university.

Table of contents

1 Introduction

1.1 Motivation / background

According to the IPCC5 report by Collins, et al. (2013) the emissions of greenhouse gases will continue to increase during the 21st century. The expected increase in greenhouse gases will lead to an increase in global temperature. However, not only the temperature will increase but also the location and amount of precipitation will change in many regions (Collins, et al., 2013). The precipitation in the Arctic region increases by more than 50 % in the RCP 8.5 scenario in some areas as shown in Figure 1.

According to Dixon, Delworth, Spelman, & Stouffer (1999) and Collins, et al. (2013) the Atlantic meridional overturning circulation (AMOC, also known as the Atlantic part of the global conveyer belt) will decrease in strength. The AMOC transfers large amounts of warm and saline waters from the equator towards the poles. While flowing towards the poles, heat is released into the atmosphere. If the AMOC strength decreases, there is less water flowing towards the poles, this means that there is less heat which can be released into the atmosphere which results in colder climates in the mid latitudes.

A process that is thought to drive the AMOC is convection in the Nordic Seas (Greenland Sea, Iceland Sea and Norwegian Sea) and Labrador Sea. Most of the heat loss to the atmosphere takes place in these regions due to the circulation of the water in gyres, which results in extra cooling. This cooling of the water makes it denser. The densification triggers the convection, the waters get dense, sink, mix vertically and spread in the intermediate and deep layers of the ocean.

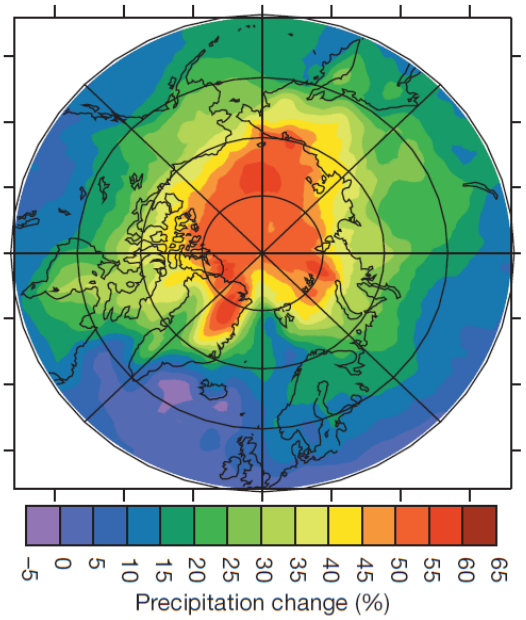

Figure 1 – Simulated changes in precipitation over the Arctic region (difference between 2091-2100 average and 2006-2015 average) in the RCP 8.5 scenario, from Bintanja & Selten (2014)

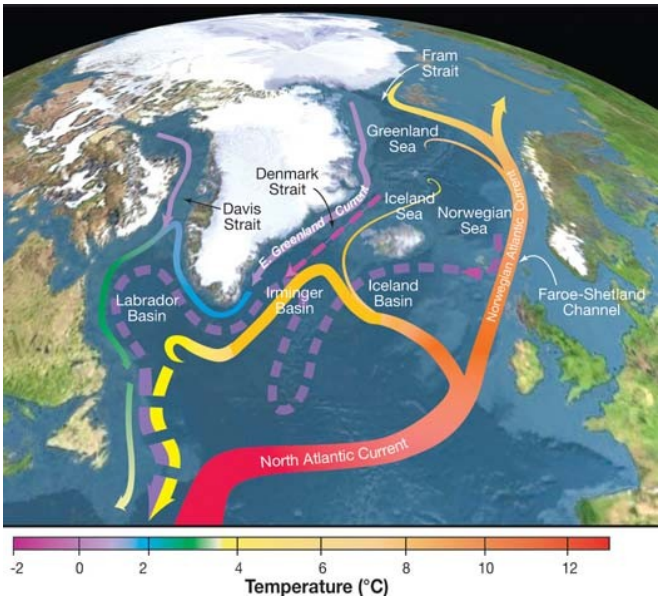

Figure 2 - Overview of the North Atlantic region with surface currents (solid curves) and deep currents (dashed curves) from (Curry, 2012)

Bintanja & Selten (2014) state that the increase in precipitation in Figure 1 may contribute to the projected weakening of the AMOC. The increase in precipitation causes the surface layer of the Arctic Ocean to become fresher. This relatively fresh water will flow from the Arctic Ocean towards the North Atlantic Ocean via Fram Strait following the ocean currents (Masson-Delmotte, et al., 2013) as shown in Figure 2. If these ocean currents stay at the same location during the 21st century, the relatively fresh surface water will reach the convection regions in the Nordic Seas and the Labrador Sea via the East Greenland Current as shown in Figure 2.

The relatively fresh water as a result of an increase in precipitation in the Arctic has a lower density and will create a layer of relatively light surface water that floats on top of the denser waters. The atmospheric cooling which will continue to occur may not be sufficient to make the density of the surface layer large enough for deep convection to occur. The decreasing amount of convection means that there is less water sinking to the intermediate and deep layers of the ocean. Less dense water in the intermediate and deep layers of the ocean means that there is also less spreading of the dense water which is thought to be one the driven processes of the AMOC (Olbers, Willebrand, & Eden, 2012).

To find out if the sea surface salinity and AMOC are indeed affected by an increase in precipitation above the Arctic Ocean Bintanja & Selten performed a model run in which the precipitation over the Arctic Ocean (above 70 degrees North) was increased with 50 %, all the other forcing factors were the same as for the present day climate; this is further explained in section 3.3. From this run with a 50 % increased precipitation above the Arctic they conclude that about 25 % of the decrease in sea surface salinity in the RCP 4.5 and RCP 8.5 scenarios can be attributed to the increased precipitation in the Arctic. This means that an increase in precipitation is an important factor in future climate change. Other mechanisms that cause the sea surface salinity in the Arctic to change are local evaporation, increased river discharge and runoff, sea-ice melt and a change in ocean advection and mixing (Bintanja et al., 2013).

In a set of similar model runs, the Arctic precipitation changes of -50 %, +50 %, +100 % and +300 % were applied to the Arctic Ocean to study the impacts of these precipitation changes in the AMOC (Bintanja & Selten, 2014). They conclude that a 50 % increase in precipitation in the Arctic leads to a decrease of around 10 % in AMOC strength. In the RCP8.5 run performed with the same climate model (EC-Earth, see section 3.2), the AMOC strength decreased with 25 %. The CMIP5 model-average for the RCP 8.5 scenario displayed a decrease of 40 % according to the IPCC5 report (Collins, et al., 2013).

In this report, the model runs performed by Bintanja & Selten (2014) are analyzed further to gain more insight in how the Arctic precipitation changes lead to a weakening of the AMOC.

1.2 Problem definition

Since the increase in precipitation in the Arctic region could cause a decrease in strength of the Atlantic meridional overturning circulation it is important that the processes involved in a decrease in strength of the AMOC are known. This research focuses on the changes occurring in the dense water formation and sinking processes in the North Atlantic Ocean as a result of a freshwater flux in the form of extra precipitation in the Arctic.

1.3 Research goal

The research goal of this graduation project is to describe and explain the effect of an extra freshwater flux (due to extra precipitation) in the Arctic region on the sinking in the North Atlantic Ocean and to relate this to the decrease of the AMOC.

1.4 Research questions

Main question:

What is the effect of an increase in precipitation in the Arctic region on the Atlantic meridional overturning circulation?

Sub questions:

- How sensitive is the strength of the AMOC to the intensity of precipitation in the Arctic region?
- How does the sea surface salinity anomaly propagate towards the convection regions?
- How does the change in convection as a result of an increase in precipitation in the Arctic affect the strength of the Atlantic meridional overturning circulation?
- What is the relationship between sinking in the North Atlantic Ocean and the strength of the AMOC?
- How does the AMOC respond to a more centered increase in precipitation in the Arctic region above 80 °N?

1.5 Reading guide

In the next chapter, chapter 2, a theoretical background is given, this includes a background on long term climate change and a theory about convection / sinking. In chapter 3 the approach for the research and the used model and model runs are described. In chapter 4 all the results of the study are shown which lead to the answer of the research questions. Chapter 5 is the discussion about the used method and the assumptions which have been made. The final chapter is the conclusions and recommendations for further research.

2 Theoretical background

In the theoretical background information about relevant topics is discussed. It is important to understand how long term climate research works and where the increase in precipitation originated from. Besides long term climate change, also some basic processes like convection and sinking are explained. These processes are important to understand since these contribute to the directly influence the Atlantic meridional overturning circulation.

2.1 Long term climate research

Modelling long term climate change is a complicated process. There are many forcings on which the climate depends. Examples of these forcings are future emissions of greenhouse gases, aerosols and other natural and man-made forcings (Collins, et al., 2013). To be able to study the future climate in different climate models, a set four consistent climate scenarios is developed by the Integrated Assessment Modelling Consortium (IAMC). These climate scenarios consist of so-called Representative Concentration Pathways (RCPs) which represent the climate forcings by greenhouse gases and aerosols. These climate scenarios are developed for use in the Coupled Model Intercomparison Project Phase 5 (CMIP5). The CMIP5 is a standard experimental protocol for studying the output of coupled atmosphere-ocean general circulation models. By this framework models results can be analysed by scientists in a systematic way.

In the CMIP5, the response of the climate to the RCP scenarios is modelled in different models. This is done because each model has a different response to the forcings and natural climate variability. This is a result of various plausible numerical representations, solutions and approximations for modelling the climate system. Together the models give information about the response of the climate to different scenarios and so insight is gained in the uncertainties of climate change (Collins, et al., 2013).

The RCP scenarios are based on two main developments: the socioeconomic development and the development of the physical system (natural fluctuations in greenhouse gas concentrations). The socioeconomic development (human behaviour) is the most unpredictable of the two and it is expected to be dominant development, above the development of the physical system. This is because human behaviour like policy choices and long term technological advances are impossible to predict. Unlike the socioeconomic development, scientists are able to calculate the main internal fluctuations of the physical system using equations of fluid motion. However, many small scale processes cannot be described by equations due to a lack of computational ability or a lack of scientific understanding (Collins, et al., 2013).

The four RCPs are consistent sets of future projections of the components of radiative forcing and together they span the full range of emission scenarios in the literature for land use and emissions of air pollutants and greenhouse gases. The four scenarios include one mitigation scenario leading to a very low forcing level (RCP2.6), two medium stabilization scenarios (RCP4.5/RCP6) and one very high baseline emission scenarios (RCP8.5) (Collins, et al., 2013).

2.2 Climate change in the Arctic

Mean global surface air temperatures are expected to increase in the 21st century. Especially the Arctic latitudes are expected to warm. A mean temperature increase of 2.2 °C in RCP 2.6 to 8.3 °C in RCP 8.5 by the end of the 21st century is projected. This is 2.2 – 2.4 times the global mean warming

projected for these scenarios (Collins, et al., 2013). The relatively large increase in temperature in the Polar Regions is called polar amplification. Polar amplification in the Arctic occurs mainly because of melting sea ice. This melting of the sea ice decreases the reflection of solar radiation (decrease in albedo). As a result, the air temperature rises and the ocean will absorb more heat. The heating of the ocean will contribute further to the sea ice melting. Also the snow cover on the continental parts of the Arctic region is expected to decrease, which will affect the surface albedo (Masson-Delmotte, et al., 2013). The polar amplification mostly occurs in the Arctic. This is because of the deep ocean mixing in the Southern Ocean which allows the ocean to take up large amounts of heat from the atmosphere which cools the atmosphere. Also the land ice on the Antarctic is much thicker than the sea ice in the Arctic, this makes that it takes much more time to melt and affect the albedo (Collins, et al., 2013).

Due to the atmospheric warming over the past decades the Arctic sea ice extent has decreased by 3.8 % per decade since 1979. The amount of ice at the end of the summer shows a decline of 11 % per decade. Since 1979, around 17 % of the perennial sea ice (1 year old sea ice) has melted or has been exported out of the Arctic basin per decade. The sea ice drift in the Arctic has a clockwise circulation pattern. That is, ice from the Siberian regions is exported through Fram Strait into the North Atlantic Ocean (Vaughan, et al., 2013).

Not only will the temperature increase and the amount of sea ice decline in the Arctic. Also the amount of precipitation is expected to rise in the 21st century. The atmosphere can hold around 7 % more water vapour per degree warming (Collins, et al., 2013) according to the Clausius-Clapeyron relation:

Equation 1

$$\frac{de_s}{dT} = \frac{L_v(T)e_s}{R_v T^2}$$

Where e_s is the saturation vapour pressure, T is the temperature, L_v = the specific latent heat of evaporation of water and R_v is the gas constant of water vapour.

Although the amount of water vapour is expected to increase significantly, the precipitation will only increase around 1.6 to 1.9 % °C^{-1} globally. In the Arctic the mean precipitation sensitivity will be around 4.5 % °C^{-1} (Bintanja & Selten, 2014). Above the Arctic Ocean peaks of an increase of precipitation of more than 50 % are modelled in the RCP 8.5 scenario (Collins, et al., 2013) as is shown in Figure 1. Bengtsson, Hodges, Koumoutsaris, Zahn, & Keenlyside (2011) state that the increase in precipitation is mostly caused by an increased poleward moisture transport. Bintanja & Selten (2014) however, state that local surface evaporation from the melting sea ice is the major cause of this precipitation increase.

2.3 Deep ocean convection

Convection is the sinking of surface waters to the intermediate and deep layers of the ocean. This phenomenon is mostly caused by the cooling of surface waters, which leads to static instability and subsequently convection. These convection regions occur in a limited amount of locations, where atmospheric and oceanic circumstances are favorable. Convection in the Atlantic Ocean is known to occur in the Labrador Sea and the Nordic Seas as shown in Figure 4Figure 5. Other locations where open ocean convection occurs are the Mediterranean Sea (Marshall & Schott, 1999) and the Weddell Sea (Robertson, Visbeck, Gordon, & Fahrbach, 2002). In the Nordic Seas, the Labrador Sea and the Weddell Sea convection occurs because of heat exchanges with the atmosphere, the convection in the Mediterranean Sea is a result of large amounts of evaporation which leads to dense, saline waters.

Figure 4 shows the two main characteristics of convection regions, the interior of the convection region and the cyclonic boundary current. The cyclonic boundary current consists of relatively warm water, in the Nordic Seas this water is provided by the Norwegian Atlantic Current and in the Labrador Sea this water is provided by the East Greenland Current. These currents will form the cyclonic boundary currents surrounding the interior of the convection regions. Heat from the boundary current is advected towards the interior of the convection region by mesoscale eddies. In the winter this interior water cools down and deep convection occurs (Drijfhout, Marshall, & Dijkstra, 2013). In late spring, when there is not enough cooling anymore, the eddies that advect the relatively warm water towards the interior make that restratification occurs (Katsman, Spall, & Pickart, 2004). The process of convection is explained in more detail in the following section.

2.3.1 Convection

Convection in the interior of the convection region (open-ocean convection) consists of three phases: preconditioning, deep convection and spreading and restratification. In the preconditioning phase the presence of a cyclonic boundary current enables weakly stratified water of the interior to get close to the surface (Androsov, Rubino, Romeiser, & Sein, 2005). The preconditioning has a scale in the order of 100 km (Marshall & Schott, 1999). When the surface water in the interior region cools (due to winter cooling), it gets denser, less buoyant and deep and intermediate convection will occur (Iovino, Straneo, & Spall, 2008). The individual plumes of the deep convection only have a relatively small diameter in the order up to 1 km with sinking velocities up to 10 cm s^{-1}. The sinking of these plumes is associated with turbulent mixing, which will create large areas with a large mixed layer depth (mixed patches) (Marshall & Schott, 1999). After the convection, the water will spread and set the water mass characteristics in the intermediate and deep layers of the ocean (Olbers, Willebrand, & Eden, 2012). Convection is observed to reach depths of 1500 m(Lilly, et al., 1999) The mixed water will disperse at intermediate and deep layers under the influence of gravity and rotation.. After a few weeks to months the mixed layer will slowly get restratified while relatively dense water still exists in the intermediate and deep layers (Marshall & Schott, 1999). The different phases of open ocean convection are shown in Figure 3.

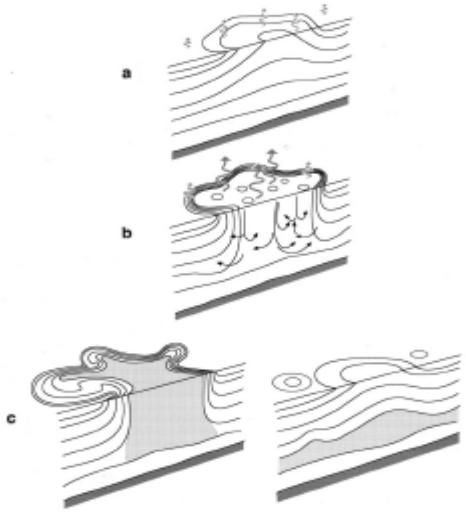

Figure 3 - Different phases of open ocean convection: (a) Preconditioning, (b) deep convection and (c) spreading and restratification (Marshall & Schott, 1999)

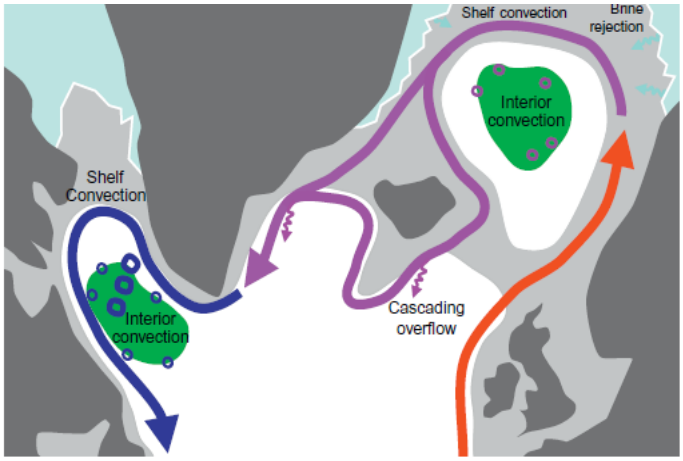

Figure 4 - Locations of the convection regions in the North Atlantic (Drijfhout, Marshall, & Dijkstra, 2013)

Although open ocean convection is associated with dense water formation it is however, not associated with significant amounts of vertical mass transport. The downward vertical mass transport within convective plumes in open ocean convection is almost completely balanced within the convection region (Marshall & Schott, 1999; Spall & Pickart, 2001; Olbers, Willebrand, & Eden, 2012).

Spall & Pickart (2001) presented a theory for the sinking of dense waters in the ocean. They show that, when it is assumed that the large-scale interior flow is governed by planetary geostrophic dynamics, a net vertical transport of water at mid-ocean is associated with a much larger horizontal mass flow. If all the sinking of dense waters that constitutes the AMOC would occur at mid-ocean, this horizontal flow would be unrealistically strong.

This theory starts with the Sverdrup relation which is derived from the linear vorticity equation, and is valid under geostrophic conditions. This equation yields a relation between the northward horizontal flow and the downward flow:

Equation 2

$$f\frac{dw}{dz} = \beta v$$

Where:

- $f = 2\Omega \sin\varphi$ = Coriolis parameter (s^{-1}), Ω is the rotation rate of the earth $(7.2921 * 10^{-5} rad/s)$ and φ is the latitude
- $\beta = \frac{2\Omega \cos\varphi}{a}$ = Rossby parameter with a = mean radius of the earth (m)
- w = Flow velocity in vertical direction (m/s)
- z = Depth (m)
- v = Flow velocity in horizontal direction (m/s)

When linearity is assumed, $\frac{dw}{dz}$ will have a uniform value of $\frac{w}{h}$ in the case of a mixed layer, so the equation becomes:

Equation 3

$$v = \frac{fw}{\beta h} \rightarrow w = \frac{v\beta h}{f}$$

Where h is the mixed layer depth. This balance requires that any sinking (w) has to be compensated with a meridional northward flow (v).

If the sinking occurs in a region with a zonal length scale of L_x and a meridional length scale of L_y, the total downward mass transport $(M_I)$is given by:

Equation 4

$$M_I = wL_xL_y \rightarrow M_I = \frac{v\beta h}{f} * L_xL_y$$

Where $L_x$and L_y are respectively zonal and meridional length scales of the region of deep mixing and sinking.

In a rectangular box, the total meridional transport (M) associated with the sinking can be calculated with:

Equation 5

$$M = hL_xv$$

If these equations are combined, this gives the ratio between M_l and M:

Equation 6

$$\frac{M_I}{M} = \frac{\beta L_y}{f}$$

If this equation is filled in with reasonable values, it turns out that the horizontal transport has to be many times larger than the vertical transport. For example, the latitude of the Labrador Sea is around 60 °N and the Nordic Seas are around 75 °N, this gives values of $f = 1.3 * 10^{-4}$ and $\beta = 1.1 * 10^{-11}$ and $f = 1.4 * 10^{-4}$ and $\beta = 5.9 * 10^{-12}$ respectively. Values L_y are in the order of 100 km (Marshall & Schott, 1999), this gives:

$$\frac{M_I}{M} = \frac{1.1 * 10^{-11} * 10^5}{1.3 * 10^{-4}} = 0.008$$

And

$$\frac{M_I}{M} = \frac{5.9 * 10^{-12} * 10^5}{1.4 * 10^{-4}} = 0.004$$

This shows that an unrealistically large horizontal overturning should exist if net sinking would occur in an area in geostrophic balance (Spall & Pickart, 2001).

So, deep convection does not feed the AMOC directly since no net mass fluxes occur. However, the intermediate and deeper layers of the Nordic Seas are filled with dense water because of this process. This results in overflow at the Greenland Scotland ridge as small-scale gravity-driven flow and then sinks. This provides an initial branch of the AMOC (Olbers, Willebrand, & Eden, 2012).

Boundary convection is the other type of convection mentioned previously. If the water in the boundary layer cools down enough, the waters in the boundary current can become baroclinically unstable. This instability results in boundary convection. The convection in the boundary current it not as deep as in the open ocean, this is because of the bottom boundary.

2.3.2 Net sinking near lateral boundaries

Besides convection in the boundary current there could also be net sinking in the boundary current as a result of horizontal density differences.

The boundary makes that there the friction which is neglected in the geostrophic balance cannot be neglected anymore. As a result Equation 2 is no longer valid. In this case horizontal advection of density is balanced by buoyancy loss to the atmosphere and convective mixing as shown in equation Equation 7 (Spall & Pickart, 2001):

Equation 7

$$u\rho_x + v\rho_y = Q$$

Where:

- Q = Buoyancy loss to the atmosphere and convective mixing
- $u\rho_x$ = The density advection in x-direction
- $v\rho_y$ = The density advection in y-direction

The buoyancy loss triggers a cooling spiral which is analogous to an Ekman spiral adjacent to the coast (Spall & Pickart, 2001). In combination with a (in this case northern) lateral boundary the horizontal flow velocity in y-direction can be approximated by:

Equation 8

$$v(z) \approx \frac{ghQ}{2\rho_0 fV}\left(1 - \frac{2z}{h}\right)$$

Where:

- Q = Buoyancy loss
- g = Gravitational acceleration $(m\ s^{-2})$
- f = Coriolis parameter (s^{-1})
- ρ_0 = Reference density of seawater $(kg\ m^{-3})$
- h = Mixed layer depth (m)
- v = Flow velocity in y-direction $(m\ s^{-1})$ as a function of depth
- z = Depth (m)
- V = The magnitude of the flow in y-direction $(m^3\ s^{-1}$

To find the total meridional overturning circulation M_B forced by sinking near the boundary can be found by integrating this equation horizontally and vertically, this resulted in:

Equation 9

$$M_B = \int_0^{h/2} \int_0^{L_x} v \, dx \, dz = \frac{g \Delta \rho_B h^2}{8 \rho_0 f}$$

Where:

- M_B = Total meridional overturning forced by boundary convection
- L_x = Zonal length scale (m)
- $\Delta \rho_B$ = Density change along a lateral boundary resulting from surface cooling $(kg\ m^{-3})$

The density differences in this equation could be a result of mesoscale eddies which transfer heat from the boundary current towards the interior of the convection region (Drijfhout, Marshall, & Dijkstra, 2013) or from general cooling of the boundary current to the atmosphere.

2.4 Overflows at the Greenland Scotland Ridge

As mentioned by Olbers, Willebrand, & Eden (2012) convection and sinking fill the basin of the Nordic Seas with dense water. The water in the North Atlantic Ocean across the Greenland Scotland Ridge has a relatively low density. This leads to overflows at the Greenland Scotland Ridge.

These overflows are directly forced by density differences between the water in the Nordic Seas and the North Atlantic Ocean. Whitehead (1998) used a model that consists of two layers to describe the amount of flow over a sill. A motionless top layer with a uniform density ρ and a bottom layer with a density difference upstream of the sill and downstream of the sill. Using this model in combination with the geostrophic equation $\left(g \frac{\Delta \rho}{\rho} = f v\right)$ and the potential vorticity equation $\left(\frac{dv}{dx} = -f\right)$ Whitehead (1998) found the following equations to describe the maximum amount of volume flux over a sill for a rectangular opening:

Equation 10

$$Q = g \frac{\Delta \rho}{\rho} * \frac{h_u^2}{2f} \quad if \quad L > \left(\frac{2g \frac{\Delta \rho}{\rho} h_u}{f^2} \right)^{1/2}$$

Or if L does not meet the condition:

Equation 11

$$Q = \left(\frac{2}{3}\right)^{3/2} L \sqrt{g \frac{\Delta \rho}{\rho}} \left[h_u - \frac{f^2 L^2}{8 g \frac{\Delta \rho}{\rho}} \right]^{3/2} \quad otherwise$$

With:

- Q = Volume transport over the sill $(m^3 s^{-1})$
- g = Gravitational acceleration $(m\ s^{-2})$
- ρ = The density in the top layer $(kg\ m^{-3})$
- $\Delta\rho$ = The density differences across the ridge
- f = Coriolis parameter (s^{-1})
- h = Height of the dynamic bottom layer (m)
- L = The width of the ridge (m)

Equation 10 and Equation 11 show that the amount of overflow is directly dependant of the density differences up- and downstream of the sill. Figure 5 shows a vertical section from one basin two another. In this figure the top layer is from the bifurcation depth to the surface and the bottom layer from the sill depth to the bifurcation depth. The bifurcation depth is the depth at which the flow in the bottom layer goes down while the top layer keeps flowing horizontally. For $\Delta\rho$ The largest density difference above the sill is taken.

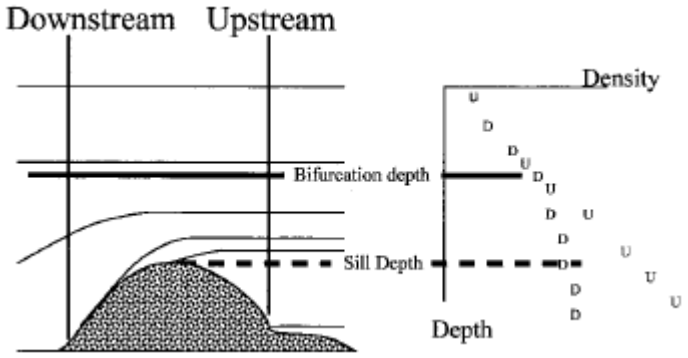

Figure 5 - Vertical section from one basin to another, D is downstream, U is upstream. The difference between D and U is $\Delta\rho$ (Whitehead, 1998)

3 Methodology

3.1 Approach

This research is based on the output of six model runs performed by Bintanja & Selten (2014). In these six runs a change in precipitation above the Arctic ranging from a decrease of 50 % to an increase of 400 % increase is modeled. The model which is used is the global climate model EC-Earth. A description of this model can be found in section 3.2 and a more detailed description of the model runs can be found in section 3.3 of this report.

With the data from the model output a sensitivity analysis is done for the sea surface salinity, mixed layer depth, which is an indicator for the amount of convection, and the Atlantic meridional overturning circulation. To find out how the sea surface anomaly propagates the correlations of the anomaly of each grid point with the anomaly at Denmark strait is calculated and maps with different time lags are created. Also the spatial changes of the mixed layer depths are plotted, this is done to see whether the convection regions change in location, this can be related to the change in sinking locations. Finally the sinking is calculated for different regions for each model run, this shows where the amount of sinking changes the most and where the decrease of AMOC strength originates from.

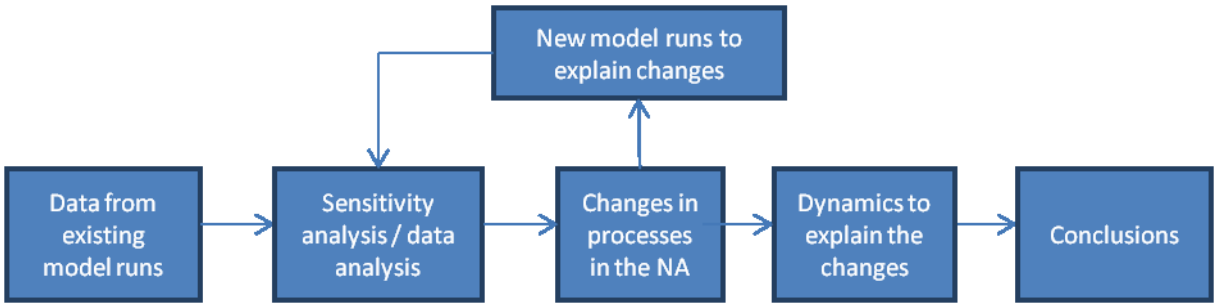

Figure 6 - Research process

3.2 EC-Earth

3.2.1 Description of EC-Earth

The model used in the research is EC-Earth. EC-Earth is a high-resolution coupled atmosphere – ocean – sea-ice – land model that has been used before in assessments, e.g. the KNMI climate scenarios and in many research projects (Sterl, et al., 2012). EC-Earth consists of three main components (Table 1).

Table 1 - Overview of used components in EC-Earth

Component	Used model	Developed by
Atmosphere	IFS (Integrated Forecast System)	European Centre for Medium Range Weather Forecasts (ECMWF)
Ocean	NEMO (Nucleus for European Modelling of the ocean)	Institute Pierre Simon Laplace (IPSL)
Sea-ice (integrated into the ocean component)	LIM (Louvain-la-Neuve Sea Ice Model)	University of Louvain-la-Neuve

The atmospheric circulation is modeled using the IFS system. The used grid size in the EC-Earth runs in this research is T159 (125 km). The IFS has 62 vertical layers from a height of 30 m to 5 hPa (≈28 km. The used time step in the IFS is 1 h (Sterl, et al., 2012).

The ocean circulation is modeled using a model component called NEMO. The basic resolution of NEMO is 1° by 1°, at the equator this is refined to 1/3°. A tri-polar grid is used with poles over North America, Siberia and Antarctica. This is done to prevent that there is a pole in the ocean, which would yield singularities in the numerical approximations. NEMO uses 46 vertical layers that increase in thickness from 6 m in the upper 15-100 m of the ocean to 300 meters is the deeper layers. The deepest layer is at 5875 m (Hazeleger & Bintanja, 2014).

Sea ice is modeled using the LIM sea ice model. It uses the same grid as the NEMO model. This model treats the sea ice as an elastic-viscous-plastic material. The dynamics are calculated by the formulation of Hunke and Dukovicz (1997) (Bouillon, Maqueda, Legat, & Fichefet, 2009). Mechanically, this models the sea ice as a two-dimensional layer that transmits stresses between the ocean and the atmosphere. From a thermodynamic perspective, it consists of an ice layer and a snow layer. These two layers have parameterizations that account for heat storage, heat conduction, snow-ice transformation, non-uniform snow and ice distributions, and albedo according to Sterl, et al. (2012)

These IFS and NEMO/LIM components are coupled by the OASIS3 (Ocean, Atmosphere, Sea Ice, Soil, version 3) coupler which is developed by the Centre Européen de Recherche et Formation Avancées en Calcul Scientifique (CERFACS). This coupler synchronizes the model components and interpolates fields between the grids. The sea-ice concentration, thickness of snow on sea ice, ice albedo and surface temperature are passed from NEMO/LIM to the IFS model. The fluxes of heat, freshwater and momentum are passed from IFS to NEMO/LIM. The used time step of OASIS3 is 3h, since this is the longest time step used in the three main components (Sterl, et al., 2012).

3.2.2 General model performance

Like every other numerical model, EC-Earth does not provide a perfect simulation of the climate behaviour. Sterl et al. (2012) compared some key oceanic variables simulated with EC-Earth and compared them with available observations to assess the performance of the model. This is done by for present-day (year 2000) forcing and pre-industrial forcing (1850) of greenhouse gases and aerosol concentrations.

The ocean temperature, salinity and sea ice extent are generally well simulated by the model. However, many areas between 40° N and 40° S are too cold and many areas outside of this region are too warm. The surface temperatures of the Irminger Sea and the Labrador Sea are about 1.5 degrees too warm. This warm bias is probably caused by a wrong position of the Gulf Stream. The Gulf Stream leaves the coast of the USA too far to the north and it is oriented too zonally. This behaviour of the Gulf Stream is characteristic for non-eddy resolving models (Sterl, et al., 2012). The warm bias in the Labrador and Irminger Seas could have an effect on the amount of convection and sinking in these regions, which could lead to a lower strength of the AMOC.

A vertical section of the salinities along 30 °W suggests that the region in which water enters the interior of the Atlantic Ocean is positioned too far to the south. A zone of too warm and saline water extends from the surface around 40 ° to a depth of 1500 m at 40 °S. This indicates that the main

convection sites are located too far to the south. A too strong outflow of the Mediterranean Sea is part of the cause according to Sterl et al. (2012). In EC-Earth the modelled outflow of the Mediterranean Sea is 1.74 Sv, while an observation-based estimate by Tsimplis & Bryden (2000) is only 0.67 Sv.

The mixed layer depths in EC-Earth have a mean that exceeds 1 km south of Greenland and south of Spitsbergen. This is in line with existing observations. The locations of the deep convection regions however are not exacly as in the observations. In the Greenland Sea the convection region is too far to the north and in the Labrador Sea the convection region is too far to the southeast.

The strenght of the modelled AMOC is quite low in EC-Earth compared to other Earth System Models and observational estimates (Sterl, et al., 2012). Under Present day conditions the AMOC is modeled to have a strength of 14.5 Sv (Sterl, et al., 2012) while the observations show an annual averaged AMOC of 18.7 Sv (Kanzow, et al., 2010). This low value of the AMOC can possibly be linked to the warm bias in the Irminger and Labrador Sea. A relatively low strength of the AMOC in the control run of this research will probably lead to a smaller effect of the change in precipitation in the Arctic region. The maximum value of the AMOC is at a depth of around 800 meters, compared to other models and observations this is too shallow (Kanzow, et al., 2010). This possible low sensitivity of the AMOC in EC-Earth is a reason to apply large precipitation anomalies in the model run that are analyzed so that a clear signal is obtained.

Sterl, et al. (2012) state that the ice distribution in the Arctic fits well to observations and estimates.

Overall the model performs quite well, however, some variables in the model are not modelled in accordance with observations. This has to be taken into account when conclusions are drawn.

3.3 Model runs

3.3.1 Description existing model runs

To study the effect of a change in precipitation in the Arctic region several model runs are performed. In these model runs the precipitation over the Arctic Ocean is changed while the forcing (emissions) are those of 2006. By using the perpetual 2006 forcing conditions, all the climate changes occurring in the model runs can be ascribed to the change in precipitation.

The six 44 year model runs (Table 2) used in this research were already performed by Bintanja & Selten (2014). Bintanja & Selten (2014) defined the Arctic region in which the precipitation is changed to be between 70 and 90 °N because most of the precipitation and sea ice changes occur in the Arctic Ocean north of 70 °N as shown in Figure 1. While the precipitation in the RCP8.5 scenario is only expected to be 150 % of the current amount of precipitation, the precipitation in the model runs in this research go up to 400 % to make changes in the system more clear.

Table 2 - Specification of model runs, the manipulation shows with what percentage the precipitation in the source code of the model is multiplied, it also shows above which latitude this is done. The percentage of precipitation is equal to αwhich is used in Equation 12. The net precipitation P_{net} is the yearly average precipitation in the region between 70° N and 90° N.

Run name	Manipulation	α	Region	P_{net} in 70N:90N	P_{net} as a percentage of P_{net} in run CTRL
P050>70	P * 50% > 70 °N	0.5	> 70 °N	$0.88*10^{12}$ m^3/year	30 %
CTRL	P * 100% > 70 °N	1.0	-	$2.92*10^{12}$ m^3/year	100 %
P150>70	P * 150% > 70 °N	1.5	> 70 °N	$4.84*10^{12}$ m^3/year	166 %
P200>70	P * 200% > 70 °N	2.0	> 70 °N	$6.76*10^{12}$ m^3/year	231 %
P400>70	P * 400% > 70 °N	4.0	> 70 °N	$13.3*10^{12}$ m^3/year	456 %
P400>80	P * 400% > 80 °N	4.0	> 80 °N	$5.29*10^{12}$ m^3/year	181 %

3.3.1.1 Manipulation precipitation in EC-Earth

As previously explained, EC-Earth consists of three parts, the IFS model for the atmosphere that calculates (amongst others) the precipitation and evaporation, the OASIS3 coupler that exchanges all variables to the NEMO model for the ocean. The manipulation of the precipitation in the model runs happened in the OASIS3 coupler. The precipitation output of the IFS model is redefined by multiplying it with a factor α:

Equation 12

$$P_{OASIS3} = \alpha * P_{IFS}$$

Where P_{OASIS3} is the net precipitation as OASIS3 passes it to NEMO, P_{IFS} is the net precipitation calculated by IFS and α is a factor with which the precipitation is multiplied. This manipulation is only done for grid points above the ocean in 70 °N - 90 °N for runs P050>70, P150>70, P200>70, P400>70 and in 80 °N - 90 °N for run P400>80. The values of α in the different runs are shown in Table 2.

3.3.1.2 Calculation of extra net precipitation relative to the control run

Since run P400>80 has a smaller region over which the precipitation is manipulated, the runs cannot be scaled to each other using α. To be able to compare the runs it is necessary to know how much precipitation is extra net precipitation compared to the control in the area above 70 °N.

EC-Earth only gives the precipitation which is calculated by the IFS model before the manipulation in m/s for each grid point per time step. This is converted to an average value in $m/year$ over the whole period (2006-2049) for each grid point. For all the grid points above the ocean the precipitation is multiplied by factor α using Equation 12 and subsequently the weighted sum of the precipitation for the whole area is taken using an integral over the area of the grid point:

Equation 13

$$P_{Tot} = \int_{70\text{N}}^{90N} \int_{0E}^{360E} P(x,y)\, dxdy$$

Where P_{Tot} is the yearly averaged precipitation in the area above latitude 70 °N in $m^3/year$. $P(x,y)$ is the precipitation calculated by IFS for a certain grid point (at location (x,y)) which is multiplied by α.

The evaporation (E_{Tot}) is calculated in the same way, except that the evaporation as calculated by IFS is not multiplied by α:

Equation 14

$$E_{Tot} = \int_{70\text{N}}^{90N} \int_{0E}^{360E} E(x,y)\, dxdy$$

This gives a total net precipitation above 70 °N of:

Equation 15

$$P_{net} = P_{Tot} - E_{Tot}$$

For run P400>80 the total amount of precipitation is calculated in the same way, however, in that only the region between 80 °N and 90 °N is multiplied by α.

The total amount of net precipitation relative to the control run in $m^3/year$ is shown in Table 2 for all simulations.

3.3.2 Description extra model runs

In the existing runs performed by Bintanja & Selten (2014) there is only one model run in which the change in precipitation is located in the region between 80 and 90 °N. Shown in Table 2 is that the extra precipitation in m^3/year on the Arctic in run P400>80 is close to the amount of extra precipitation in run P150>70. Since the increase in precipitation in run P400>80 is a relatively small amount compared to the precipitation in the runs above 70 degrees north, there is a chance that there is hardly any effect to the AMOC. To make the effects more clear an extra model run (NPE946>80) is performed in which the total precipitation is comparable to model run P400.

Since not only the precipitation but also the evaporation is expected to increase in the 21st century, the net precipitation is increased in the new runs instead of only the precipitation as is the case in the runs performed by Bintanja & Selten (2014).

Before the new model runs are conducted, it is necessary to perform a new control run and a new reference run in which the precipitation is 400 % in the 70 -90 °N region to know what the amount of precipitation is which have to be applied in the 80 -90 °N region new run. This is done to make sure that the settings and conditions in the runs are consistent with the control run and make the runs comparable.

In model run NPE946>80 the amount of extra precipitation above 80 °N it is attempted to set the extra net precipitation above 80 °N equal to the amount of extra net precipitation in NPE400>70. Since the increase of precipitation influences the climate in the model, it is not possible to get the exact same value of extra precipitation in run NPE400>70, but at least it will be approximated.

An overview of the new model runs is shown in Table 3.

Table 3 - Specifications extra model runs

Run name:	Manipulation	α	Location	P_{net} in 70N:90N	P_{net} as a percentage of P_{net} in run CTRL
NCTRL	P * 100 %	1.0	-	3.04*10^{12} m^3/year	100 %
NP400>70	P * 400 %	4.0	> 70 °N	14,5*10^{12} m^3/year	476 %
NPE400>70	(P + E) * 400 %	4.0	> 70 °N	9.76*10^{12} m^3/year	321 %
NPE946>80	(P + E) * 946 %	9.46	> 80 °N	9.16*10^{12} m^3/year	302 %

The amount of net precipitation in run NPE400>70 is calculated following the procedure described in section 3.3.1.2. The only difference is that this time also the evaporation of grid points above the ocean is also multiplied by α just as is done with the precipitation in Equation 12 before using Equation 14. This results in a net increase in precipitation of 6,72*10^{12} m^3/year compared to the new control run NCTRL. So 6,72*10^{12} m^3/year will be the amount which will be applied in the 80 - 90 °N area in the new run NPE946>80.

To determine what the value of factor α should be the following equation is used:

Equation 16

$$P_{net\ \mathrm{NPE946>80}\ Total} = P_{net\ \mathrm{NPE946>80}} + \beta * P_{net\ \mathrm{NPE946>80}}$$

Where $P_{net\ \mathrm{NPE946>80}\ Total}$ is the total amount of net precipitation in 80 - 90 °N in the new run $\mathrm{NPE946} > 80$. $P_{net\ \mathrm{NPE946>80}}$ is the amount of precipitation calculated by the IFS model and $\alpha * P_{net\ IFS}$ is the part of the precipitation which should equal 6,72*10^{12} m^3/year (the extra net precipitation) averaged over all grid points. This gives:

$$\beta * P_{net\ IFS} = 6{,}72 * 10^{12} \rightarrow \beta = \frac{6{,}72 * 10^{12}}{P_{net\ \mathrm{NPE946>80}}}$$

Since $P_{net\ \mathrm{NPE946>80}}$ is not known before the run is performed, this is approximated using the average net precipitation in the area above 80 °N for the control run, which is $7.94 * 10^{11}$ m^3/year. This gives:

$$\beta = \frac{6{,}72 * 10^{12}}{7.94 * 10^{11}} = 8.46$$

From Equation 12 and Equation 16 the relationship between α and β becomes $\alpha = \beta + 1$. This gives a value for α of 9.46. The total amount of extra net precipitation in run $\mathrm{NPE946} > 80$ is 6,12*10^{12} m^3/year as is shown in Table 3, this is smaller than 6,72*10^{12} that was strived to approximate. However, this amount is still significantly larger than 2.37*10^{12} m^3/year as in run P400>80, so it is expected that this will still give a larger signal which was the purpose of this run.

4 Results

4.1 Sensitivity analysis of the sea surface salinity, mixed layer depth and the Atlantic meridional overturning circulation

The sea surface salinity (SSS), the mixed layer depth (MLD) and the Atlantic meridional overturning circulation (AMOC) are all strongly related. The salinity of the sea surface in the Arctic Ocean will be fresher when the precipitation increases. A fresher sea surface will create more stratification in the ocean. More stratification will result in a smaller mixed layer depth. The mixed layer depth is an indicator for convection and sinking occurs in the boundary current of convection regions. Because all these variables are so strongly related, a sensitivity analysis of these variables is performed to get an overview of the strength of the responses.

4.1.1 Sea surface salinity

For the model runs in Table 2 and Table 3 the sea surface salinity in Fram, Denmark and Davis Strait is calculated. The locations of the straits are shown in Figure 7, in this figure also the mixed layer depths for the first ten years of the control run are shown which indicates convection. It is chosen to calculate the sea surface salinities in these straits because these straits are upstream of a convection region as the mixed layer depths indicate. A change in SSS upstream of a convection region will probably affect the convection which will make the salinities in these locations useful.

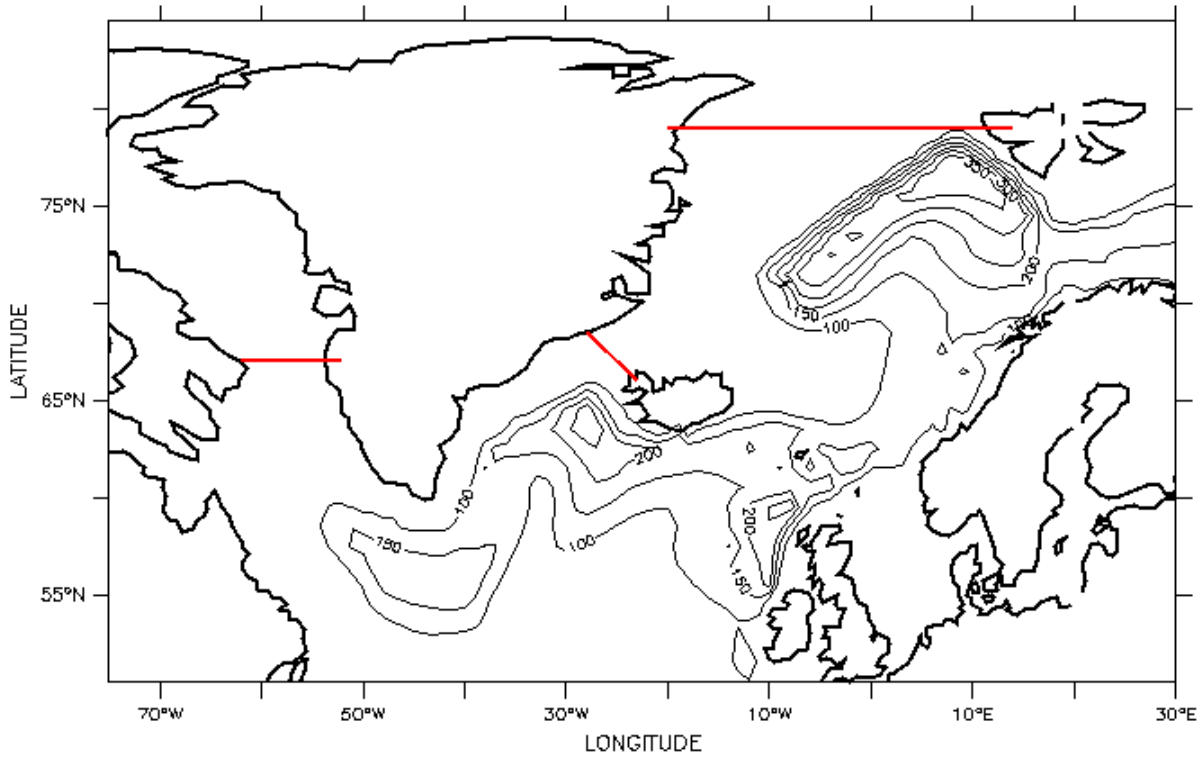

Figure 7 - Locations of Fram, Denmark and Davis Strait, also shown are the contours of the mixed layer depth (m) averaged over the first 10 years of the control run to give an indication of the convection regions. Currents are predominantly southwards through these straits.

The sea surface salinities are directly available from the output of EC-Earth. However, these are not used because the salinities at the boundaries between the ocean and the land are interpolated. The

interpolation is a side effect when the output of NEMO was regridded from the original curvilinear grid to a workable 360x180 degrees longitude-latitude grid. A drawback of the regridding is that the values on the new grid are an interpolation of the values of the curvilinear grid. Near land-sea borders this interpolation leads to lower values of the salinity since the salinity at the land is zero in the model output. A workaround for this interpolation which leads to too low sea surface salinities close to the land-sea border is to calculate the salinities using the original output on the curvilinear grid. A program called CDFtransport is used to calculate the salt and volume transport of the surface layer of the ocean. The salt transports (STRP in kT/m^3) and volume transports (VTRP in m^3/s) are used to calculate the salinities (SAL in kg/m^3) following equation:

$$SAL = \frac{STRP}{VTRP}$$

CDFtransport is part of the package CDFtools which is a package with tools written in fortran 90 specifically developed for the analysis of NEMO model output (La Forge du LEGI, 2015). The program CDFtransport uses the salinities and flow velocities that are given as output of the NEMO model to calculate the salt and volume transport. The output that this tool uses is on the original grid without a regridding transformation. Every section is divided into segments corresponding to the U or V velocity component. In this way the volume conservation is ensured and the velocities and salinities are not interpolated (Molines, Dussin, & Balmaseda, 2011).

In Figure 8 the sensitivities of the average cross section surface salinities in Davis, Fram and Denmark Strait are shown. The figure shows the sea surface salinities for the runs performed by Bintanja & Selten (2014) (>70°N solid lines and > 80°N squares) and the new model runs performed in this research (>70°N dotted lines and > 80°N triangles). The exact values of the SSS and the standard deviations can be seen in Table 9 and Table 10 in the appendix.

The figure shows that the sea surface salinities in all three straits in the model runs performed by Bintanja & Selten (2014) have a nearly linear relationship with the amount of precipitation. From these three locations, Davis Strait and Fram Strait are the most sensitive to a change in the amount of Arctic precipitation. This can be explained by the fact that the water through these straits originates directly from the Arctic. This is not the case with the water that flows through Denmark Strait: partly this is water from the Arctic via Fram Strait, but it is mixed with Atlantic water in the gyre in the Nordic Seas as shown in Figure 2. The changes in sea surface salinities in the straits relative to the control run are in the order of magnitude of +0.3 to +1.0 % for run P150>70 and +3.5 to +6.8 % in run P400>70 as shown in Table 9.

The new model runs that are performed in this research do not show a linear trend. The different responses between the model runs performed by Bintanja & Selten (2014) and the new model runs are difficult to explain. It could be that the two sets of model runs do have the same trend, but that it is not visible because of the different amount of model runs with different amounts of precipitation.

If the extra freshwater forcing is only applied to the region above 80 °N in run P400>80 and run NPE946>80, the averaged sea surface salinity at Fram Strait is clearly lower. The cause of this decrease in density is that Fram Strait is located at 80 °N with a dominant southward flow, this makes that all the extra precipitation is located upstream of Fram Strait. The East Greenland Current

transports these relatively fresh surface waters further towards Denmark Strait, which makes that the surface salinities in Denmark Strait are also lower compared to the runs where the precipitation is changed above 70 °N, however, because of mixing in the Nordic Seas the effect is less visible.

In Davis Strait the surface salinity is only a very little bit lower in run P400>80 compared to the runs where the precipitation is changed above 70 °N. This indicates that for the amount of relatively fresh water in Davis Strait it does not matter if the precipitation increase above 70 °N or 80 °N. However, the sea surface salinity in Davis Strait does not show the same behaviour in run NPE946>80 compared to the runs above 70 °N. The salinity in Davis Strait is slightly higher compared to the runs above 70 °N, this indicates that less relatively fresh water flows through Davis Strait if the precipitation is located above 80 °N.

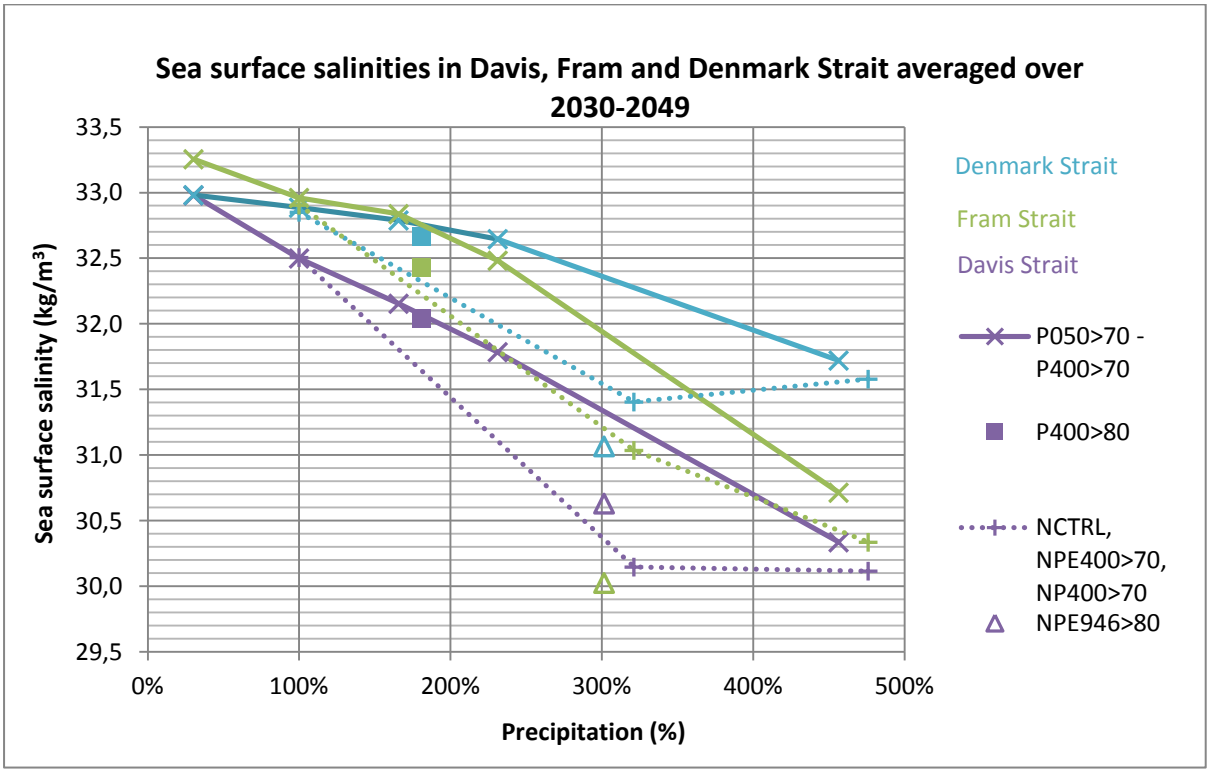

Figure 8 – Cross section averaged sea surface salinities in (purple), Fram (green) and Denmark (blue) strait for the runs performed by Bintanja & Selten (2014) (>70°N solid lines and > 80°N squares) and the new model runs performed in this research (>70°N dotted lines and > 80°N triangles) averaged over the last 20 years of the model runs

4.1.2 Mixed layer depth

The mixed layer depth gives an indication how well mixed the upper layer of the ocean is. A large mixed layer depth indicates that there is deep convection occurring. Since convection plumes have a relatively small horizontal scale on the order of 1 km (Marshall & Schott, 1999), the individual plumes are not resolved in coarse resolution models. The mixed layer depth provides a useful indication for the depths that these convection plumes reach (Paluszkiewicz, Denbo, & Garwood, 1994).

The ocean part of EC-Earth (NEMO) contains the mixed layer depth (MLD) as an output variable. The mixed layer depth is the depth at which the difference of sigma-0 (σ_0) with the surface equals 0.01 kg/m^3 (Grieco & Masina, 2009). Sigma-0 is defined as the potential density with a reference pressure of 0 (surface pressure) minus 1000 (Brown, et al., 1989). The potential density is the density

calculated using the potential temperature. This potential temperature is used because when a water parcel is moved adiabatically to a different pressure, the compression or expansion will make that the temperature of the parcel increases or decreases respectively, this change in temperature (and density) is not of interest in finding the mixed layer. The equation for sigma-0 is:

Equation 17

$$\sigma_0 = \sigma(s, \theta, 0) = \rho(s, \theta, 0) - 1000\ kg/m^{-3}$$

Here σ is an expression for the density and ρ is the absolute value of the density. For the calculation of the mixed layer depth, the densities are calculated using the salinity (s), potential temperature (θ) and a reference water pressure of 0.

The mixed layer depth is calculated for two different areas: the Labrador Sea and the Nordic Seas as shown in Figure 9. These areas are chosen since these are the primary areas where open ocean convection occurs (Drijfhout, Marshall, & Dijkstra, 2013). The areas are chosen in such a way that the larger values of the mixed layer depth are within the area in both the run CTRL and run P400>70.

For both regions, the MLD is quantified in two ways: by the maximum mixed layer depth and an average mixed layer depth. Both are averaged over the last 20 years of the model run. Since the largest mixed layer depths occur in the winter period, December - April, only the mixed layer depths in these months are taken into account. For the average mixed layer depth, the average of the areas shown in Figure 9 are taken, for the maximum mixed layer depth only the largest value in these areas are taken.

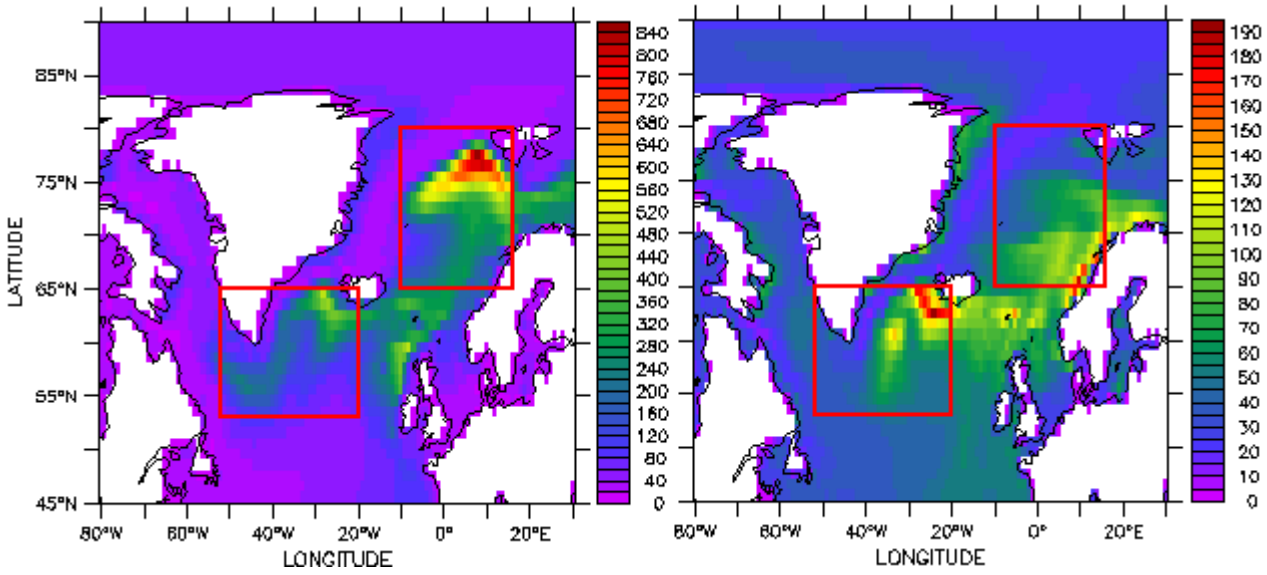

Figure 9 - Locations for which the average value of the mixed layer depths are calculated, the mixed layer depths for run CTRL and P400>70 are used as background

The results for the sensitivity analysis of the mixed layer depths are shown in Figure 10 and Figure 11. Figure 10 shows the mixed layer depths averaged over the regions shown in Figure 9. Figure 11 shows the maximum value of the mixed layer depths in those regions. The model runs performed by Bintanja & Selten (2014) above 70°N are shown with solid lines and above 80°N are shown with squares. The new model runs performed in this research above >70°N are shown with dotted lines

and above 80°N with triangles. The exact values of the SSS and the standard deviations can be seen in Table 11 to Table 14.

The figures show a decreasing trend of the mixed layer depths (MLDs) when the precipitation increases. The average MLD decreases by 6 – 12 % in run P150>70 to 62 – 73 % in run P400>70. The maximum MLD in these runs decreases by 11 – 25 % in run P150>70 to 43 – 76 % in run P400>70. The mixed layer depths decrease because precipitation makes the surface waters fresher and lighter which will prevent the occurrence of convection and thus water mass transformation. The new model runs performed in this research in which the precipitation is increased above 70 °N show roughly the same pattern as in the model runs performed by Bintanja & Selten (2014).

The mixed layer depths in the Nordic Seas are more sensitive to a change in the amount of precipitation above the Arctic than the Labrador Sea. A possible explanation could be that a large part the Nordic Seas is covered by the area above 70 °N where the amount of precipitation is changed in runs P050>70 – P400>70. The Labrador Sea is located more to the south, and before the relatively freshwater has reached this area the water mixes with water from the Atlantic with an unaltered, which results in a lower sensitivity.

For model run P400>80 the average mixed layer depths in the two areas are not much affected. The maximum mixed layer depths are slightly higher than in the runs P050>70 – P400>70. This could be because the precipitation anomaly is not directly applied above the convection region in the Nordic Seas. For the Labrador Sea the explanation could be that more the relatively freshwater has to travel further and more mixing will occur.

The average mixed layer depths in model run NPE946>80 differ slightly from the new model runs in which the precipitation is increased above 70 °N. In the Nordic Seas the mixed layer depth is slightly higher and in the Labrador Sea the MLD is slightly lower. This indicates that the Nordic Seas are less affected by the precipitation changes, this could be because the precipitation is not directly increased above the convection area in the Nordic Seas. The Labrador Sea shows a slightly smaller mixed layer depth. The maximum mixed layer depths are not much affected by the change in location of precipitation, this is consistent to the results of run P400>80.

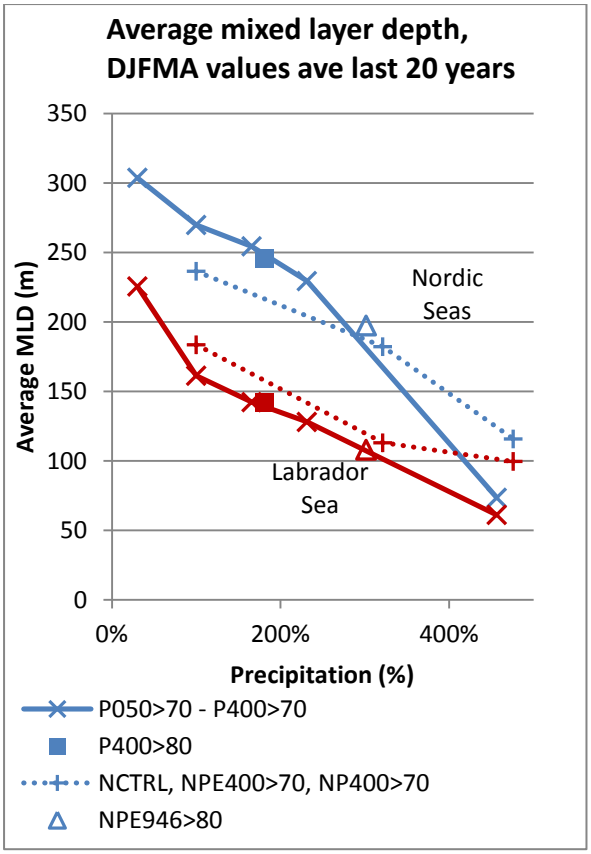

Figure 10 - Sensitivity of the average mixed layer depths, DJFMA values are averaged over the last 20 years

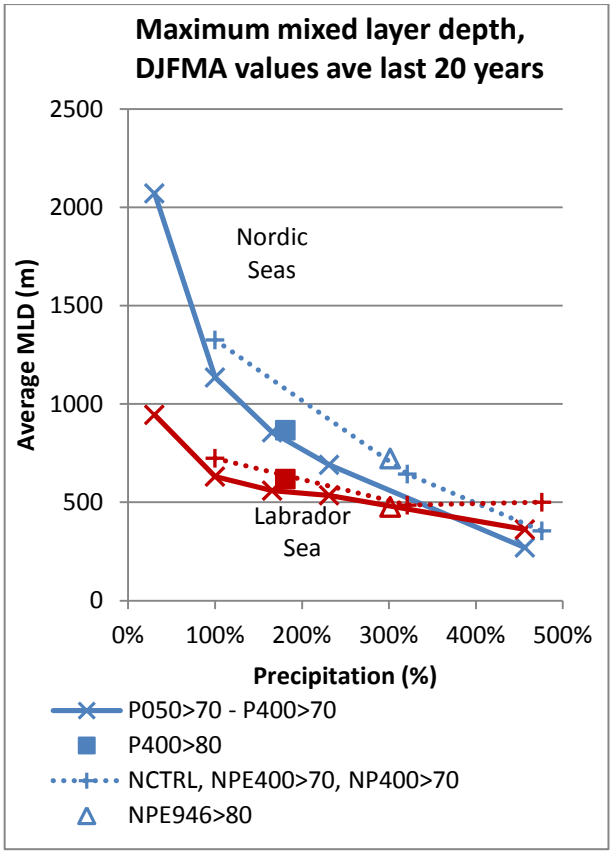

Figure 11 - Sensitivity of the maximum mixed layer depths, DJFMA values are averaged over the last 20 years

4.1.3 Atlantic meridional overturning circulation

The Atlantic meridional overturning circulation (AMOC) is the stream function of the total (basin wide) circulation in the latitude-depth plane. Where the Thermohaline Circulation is only a theoretical concept of the circulation forced by density changes as a result heat and salinity exchanges with the atmosphere, the AMOC is the total circulation in the basin including wind driven circulation of which the strength can be calculated (Drijfhout, Marshall, & Dijkstra, 2013).

The meridional overturning circulation (MOC) is computed using the program CDFmoc. This program is like CDFtransport part of the package CDFtools. This program computes the MOC by integrating the V-velocity field zonally and subsequently integrating vertically (Molines & Treguier, 2006). The definition of the AMOC is given by:

$$\psi(x,y) = \iint v\,dx\,dz$$

Where $\psi(x,y)$ is the MOC stream function, v is the yearly average of the meridional velocity, x and z are the zonal and vertical coordinates (Fischer & Jungclaus, 2010). The AMOC is the MOC calculated only in the Atlantic Ocean.

The sensitivity of the strength of the AMOC at 30 °N is shown in Figure 12. The strength of the AMOC is calculated as the maximum AMOC strength at 30 °N and is expressed in Sverdrup (Sv), one sverdrup = 10^6 m^3/s. Clearly the AMOC decreases in strength as the amount of precipitation increases. The decrease in AMOC strength for run P050>70 is around 11 %, this increases to 43 % for run P400>80.

In model run P400>80 the AMOC strength is almost the same as if it would have been the case if the same amount of precipitation would have been located in the area above 70 °N. This indicates that the AMOC is not very sensitive to the location of the precipitation, but more to the amount of precipitation. This is in line with the mixed layer depths which are also hardly affected by the location of the precipitation. Also the new model runs in Figure 12 show that the AMOC is not sensitive to the location of precipitation.

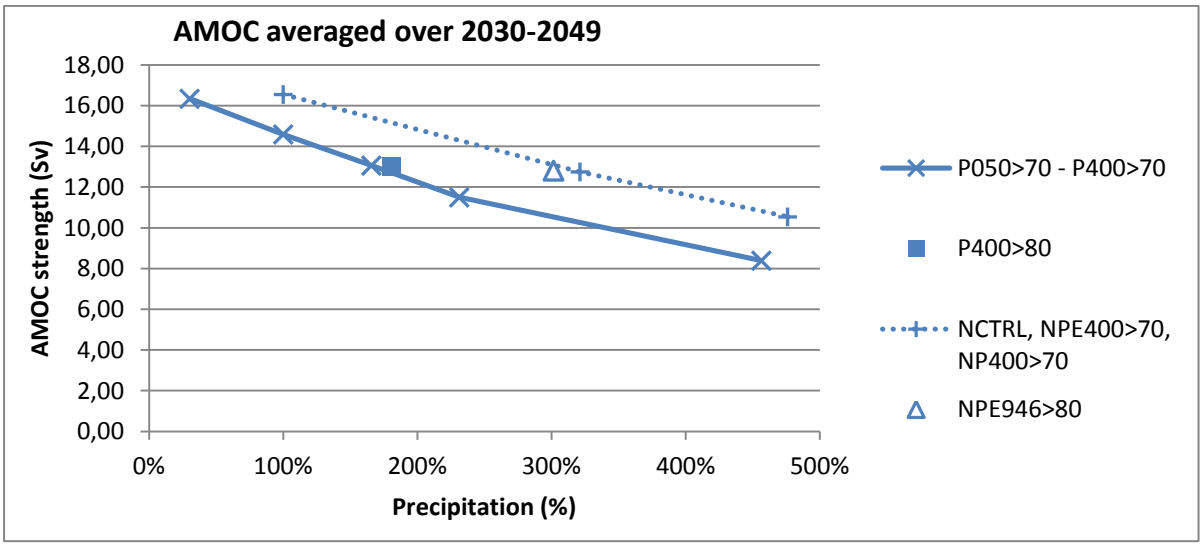

Figure 12 - AMOC strength (Sv) yearly values averaged over the last 20 years of the model runs

All variables which are analysed in this sensitivity analysis show a declining trend with an increase in precipitation. Although the sea surface salinities in runs with the precipitation anomaly applied to the region above 80 °N differ from the model runs with ΔP > 70 °N, this difference is much smaller in the mixed layer depths and the strength of the AMOC. This indicates that the amount of precipitation has more influence on the mixed layer depths and AMOC strength than the location. What the sensitivity analysis also shows is that sea surface salinities only experience small changes, but that the effect on the mixed layer depths and the AMOC are large. However, the small changes in sea surface salinity are twice as large as the standard deviation (Table 9) which shows the natural variability, this explains why a relatively small change in sea surface salinity has a large effect on the mixed layer depths and AMOC.

4.2 Salinity anomaly propagation

The modeled increase in precipitation in the Arctic region leads to a salinity anomaly propagating from the Arctic towards the North Atlantic Ocean. To visualize how the salinity anomaly propagates from the Arctic towards the cross correlation is used.

If two time series, Y_1 and Y_2 are compared and n^* is defined as the number of overlapping positions between the two time series, the cross correlation for a match position m is:

$$r_m = \frac{n * \sum Y_1 Y_2 - \sum Y_1 \sum U_2}{\sqrt{[n^* * \sum Y_1^2 - (\sum Y_1)^2][n^* \sum y_2^2 - (\sum Y_2)^2\ ]}}$$

Which is equivalent to:

$$r_m = \frac{cov_{1,2}}{s_1 s_2}$$

Where:

- $cov_{1,2}$ = The covariance between the overlapped portions of sequences Y_1 and Y_2
- s_1 and s_2 = The corresponding standard deviations (Davis, 2002).

In this case the cross correlation is used to create maps at different time lags that show the cross correlation coefficients between the sea surface salinity in one of the straits (Davis, Fram or Denmark, see Figure 7) and each individual grid point in the area of interest.

To make these maps, first a time series (Y_1) of the dSSS in the straits is extracted from the model output data:

$$dSSS = SSS_{run} - SSS_{control}$$

here SSS_{run} and $SSS_{control}$ are the time series of the the sea surface salinities in one of the straits for a specific model run and for the control run respectively. Similarly, a time series (Y_2) of the dSSS at a certain grid point is extracted from the data.

Finally the correlation between the two time series Y_1 and Y_2 is calculated. This is done for each individual grid point in the area of interest, with all these correlations a map is created. Multiple maps are created where Y_2 lags Y_1 from -5 months and +10 months to the SSS of Y_1. These maps will show where the salinity anomaly originates from and the locations where it propagates towards.

Figure 13 shows the correlation of each grid point with the average dSSS in Denmark Strait at lags of -5 months, 0 months, +5 months and +10 months. In this case salinity is used as tracer to follow the pathway that the sea surface salinity anomaly follows. Based on Figure 13 the water takes around 5 months to travel from Fram Strait (A. lag -5 months) to Denmark Strait (B. lag 0 months). It appears that there is a very low correlation of the SSS anomalies in the Nordic Seas with the SSS anomalies at Denmark Strait at a lag of -5 months as shown in Figure 13 A. After Denmark Strait the anomaly travels towards the entrance of the Labrador Sea at a lag of +5 months (C.). The weakening of the signal after Denmark Strait is a result of mixing with North Atlantic water. After ten months the anomaly exits the Labrador Sea as shown in Figure 13 D.

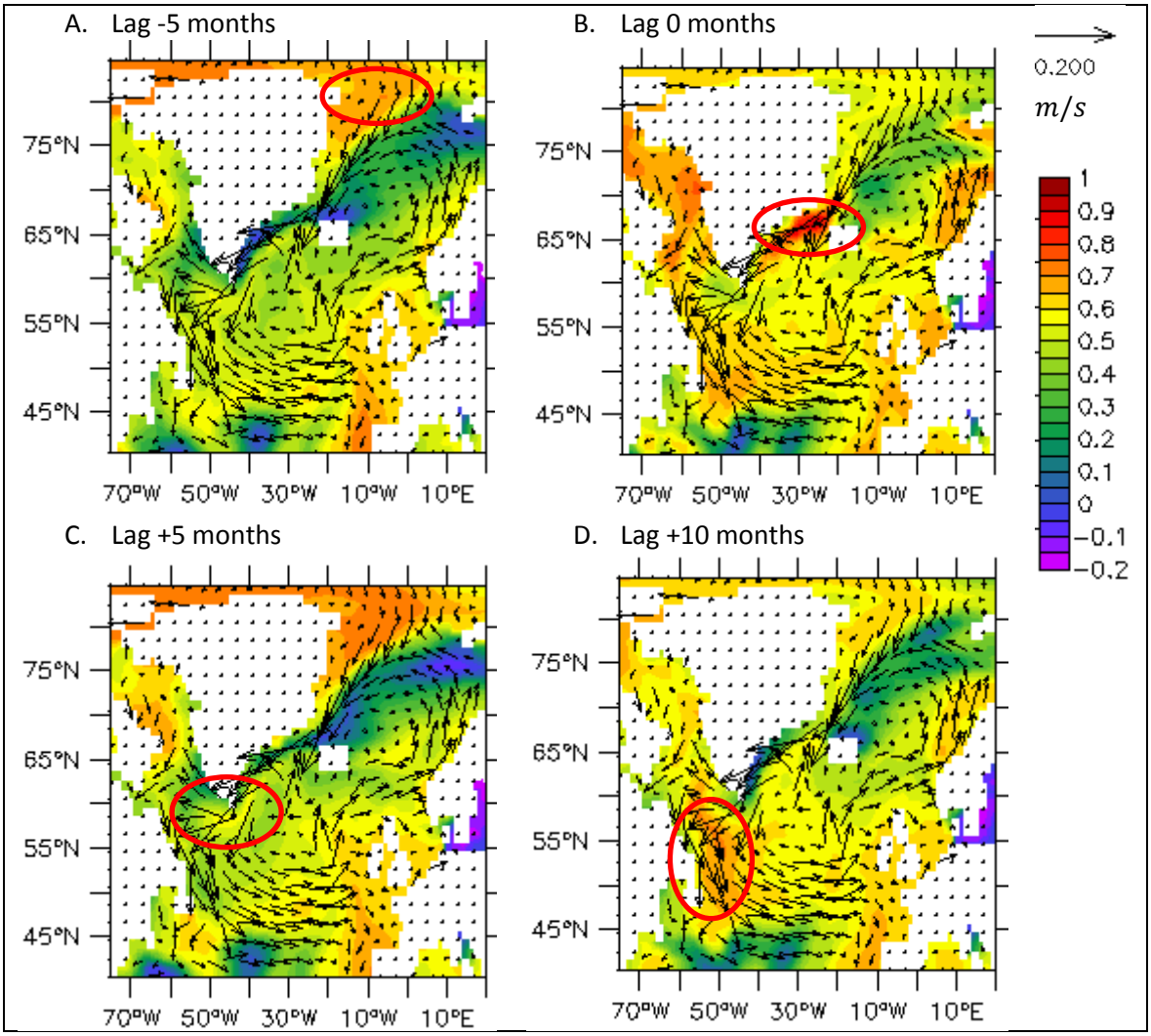

Figure 13 - Maps with correlations between dSSS at grid points vs dSSS at Denmark Strait. The salinity anomaly at the grid points has a lag between -5 months and +10 months compared to the SSS in Denmark Strait.

4.3 Spatial changes in the mixed layer depth

As stated in section 4.1.2 of the report, the depth of the mixed layer is a good indicator for the amount of convection that occurs. To be able to link the convection regions with the regions in which sinking occurs later in the report, the spatial changes of the mixed layer depth are mapped for different model runs in Figure 14. As was already mentioned by Sterl, et al. (2012) the convection region in the Nordic Seas is too far to the northeast and the convection region in the Labrador Sea is too much to the southeast compared to observations. In run CTRL (A.) this is clearly visible. These maps also show that in the model there is a convection region in the Irminger Sea near the southwest of Iceland and a convection region near the coast of Scotland. The convection region in the Irminger Sea is also observed as shown in Figure 2, however, the convection region near the coast of Scotland is not observed.

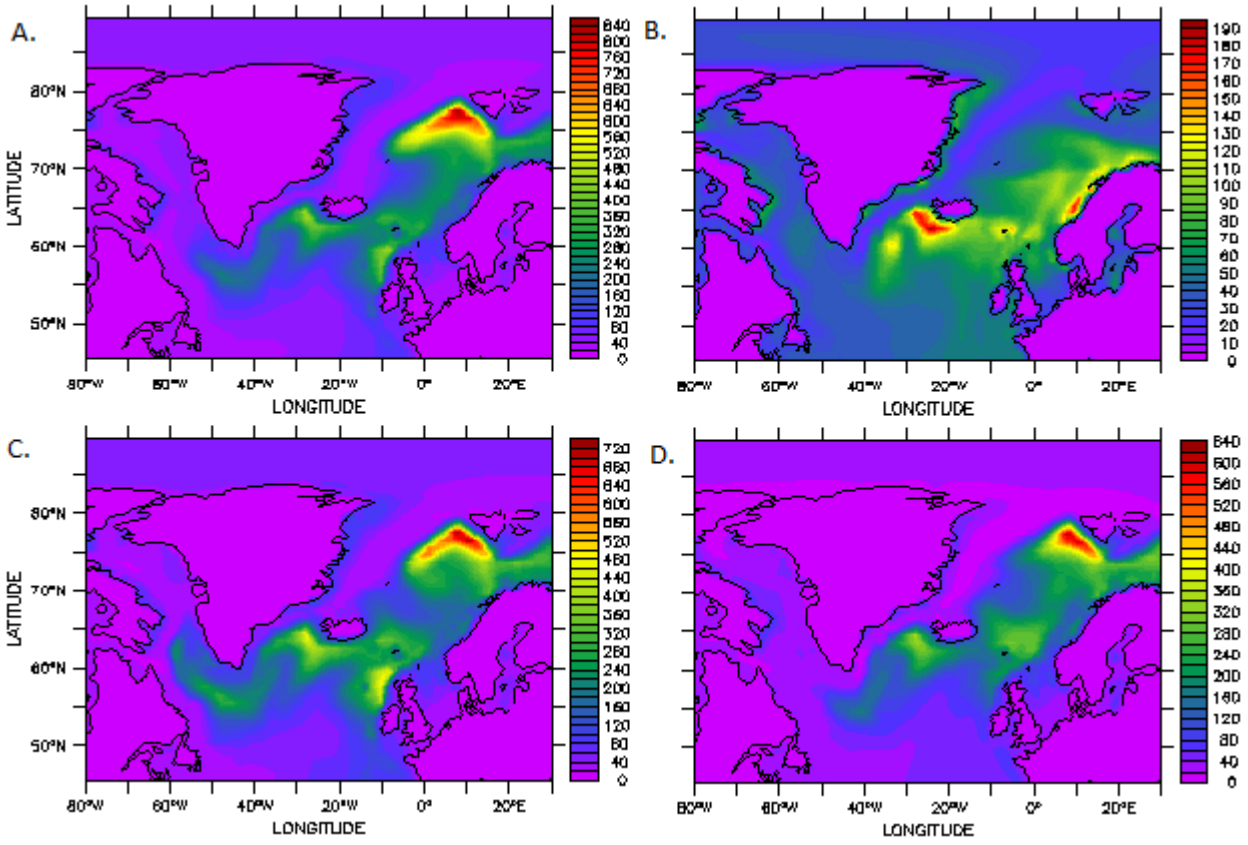

Figure 14 - Mixed layer depths, DJFMA averaged over the last 20 years of the model runs. Run CTRL (A.), run P400>70 (B.), run NCTRL (C.) and run PE946>80 (D.)

When the precipitation is increased north of 70 °N as in run P400>70 (Figure 14b), the convection region in the Nordic Sea decreases from a depth of 840 m to a depth of just 110 m. The convection region in the Labrador Sea disappears almost completely and the convection region in the Irminger Sea decreases from a depth of 450 m to a depth of 200 m. Figure 15 shows the density profiles in the Labrador Sea, the Irminger Sea and in the Nordic Seas. The specific locations are shown in Figure 30 in the appendix. The density profiles shown that in the Labrador and Nordic Seas indeed a layer of relatively freshwater floats on top of the denser water, the surface densities decreased with more than 1 kg/m^3 from run CTRL to run P400>70. In the Irminger Sea the decrease of surface density is only 0.5 kg/m^3. This explains why the convection region in the Irminger Sea does not decrease as much as the other two.

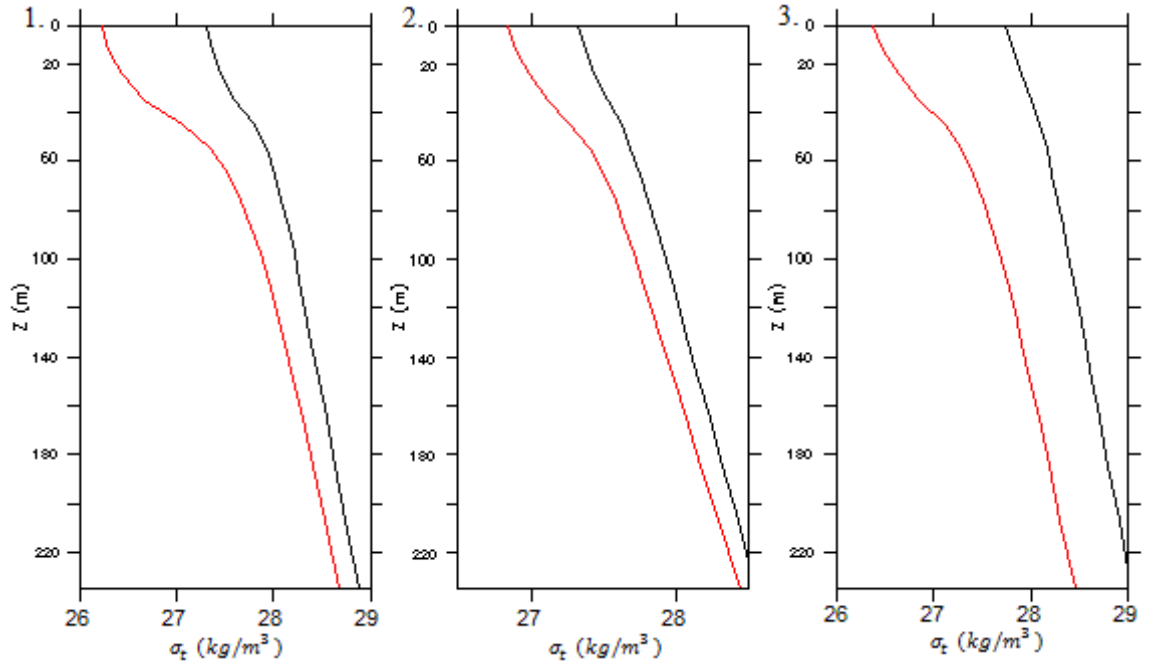

Figure 15 - Density profiles in the Labrador Sea (1), Irminger Sea (2) and Nordic Seas (3) for run CTRL (black) and run P400>70 (red)

When the precipitation is only increased above 80 °N as in run NPE946>80 the convection regions stay in the same locations as in the control run (see Figure 14 C and D). All the convection regions slightly decline in depth, but not nearly as much as in run P400>70. The density profiles in Figure 16 show that the surface density decreased with only 0.15 kg/m^3, also the densities at larger depths decreased. This makes that the vertical density gradient almost did not change and also the convection areas stayed in the same location and that the mixed layer depth only declined in strength slightly.

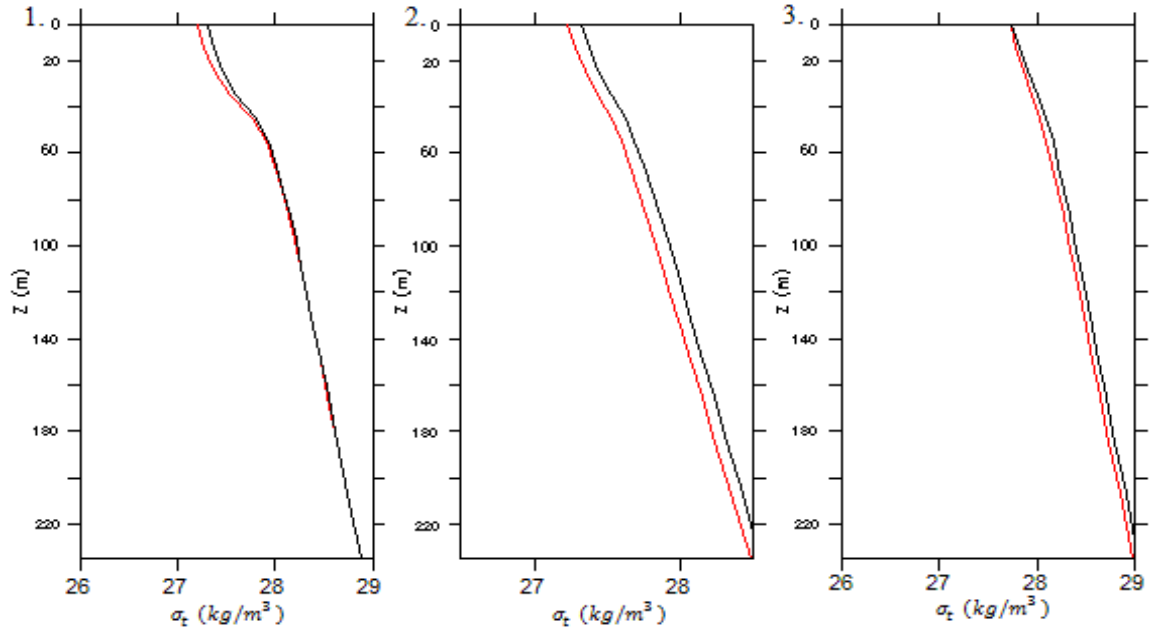

Figure 16 - Density profiles in the Labrador Sea (1), Irminger Sea (2) and Nordic Seas (3) for run NCTRL (black) and run PE946>80 (red)

4.4 Sinking

As described in section 2.3.1 of the report, according to Marshall & Schott (1999) the role of open ocean convection plumes is not significant in vertical mass transport. According to the theory as described in the literature review in section 2.3.2 the main region where dense water sinks and net vertical mass transport occurs is in a narrow strip along the perimeter of the marginal seas. The vertical flow velocity is used to study where this net vertical mass transport occurs in the model runs and how this mass transport changes as a result of changes in precipitation above the Arctic.

In order to see how the sinking changes when the precipitation in the Arctic region is increased, the total vertical mass transport for different regions in the North Atlantic Ocean is calculated (Figure 20 and Figure 21). The vertical mass transport occurring in the North Atlantic Ocean is calculated by integrating the vertical flow velocity in the x and y direction of an area of interest:

$$Vertical\ volume\ flux\ (Sv) = \iint w\,dx\,dy$$

Where w is the vertical flow velocity (m/s), x and y are respectively the meridional and zonal direction (m).

To be able to capture the largest signal of sinking, continuity is used to find the depth at which the sinking is the largest. If the North Atlantic would have been a semi enclosed basin with only an opening to the south, from continuity it would follow that the maximum vertical mass transport should occur at the depth at which the Atlantic meridional overturning circulation has it maximum strength. However, the North Atlantic Ocean is not a semi enclosed basin: exchange of water with the Arctic Ocean can occur over the Greenland Scotland Ridge. Figure 17 shows that there is a circulation of roughly 4 Sv flowing from the North Atlantic Ocean into the Arctic Ocean at 66.5 °N, this shows that there is indeed water exchanged with the Arctic Ocean.

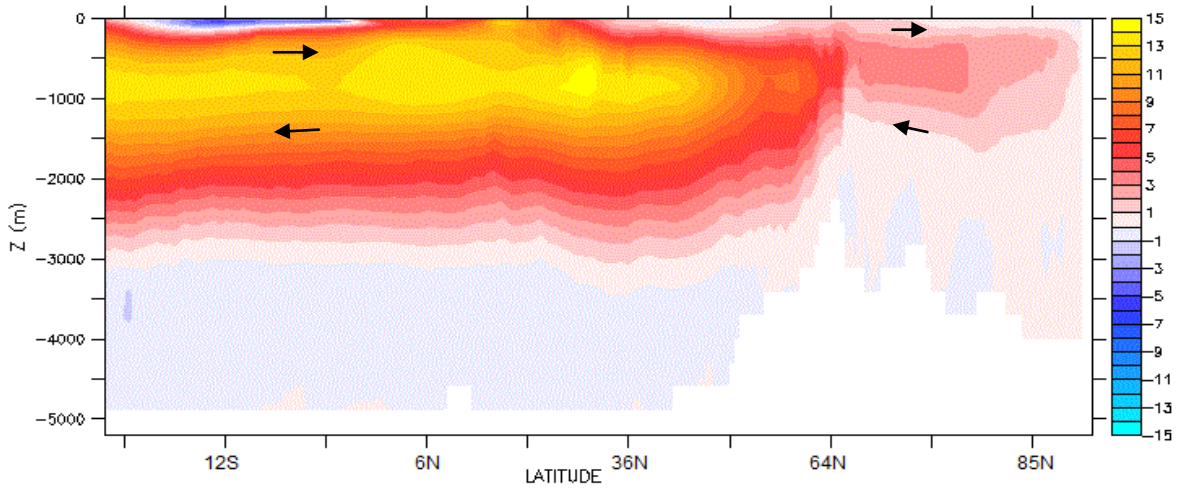

Figure 17 - Atlantic meridional overturning stream function for run CTRL

Because this is the case, this means that the maximum vertical mass transport does not necessarily occur at the depth where the AMOC has the largest strength. The maximum amount of vertical mass transport occurs at the depth where the difference between the maximum AMOC strength and the AMOC strength at 66.5 °N is the largest. This horizontal difference of the AMOC in the control run is shown in Figure 18. To exclude the effect of the wind-driven circulation at the surface, only the horizontal gradient at depths greater than 500 m are taken into account. The maximum horizontal difference in all model runs turns out to have a depth of 880.5 meters as shown in Table 4. This will be the depth used for analyzing the sinking patterns in the subsequent section.

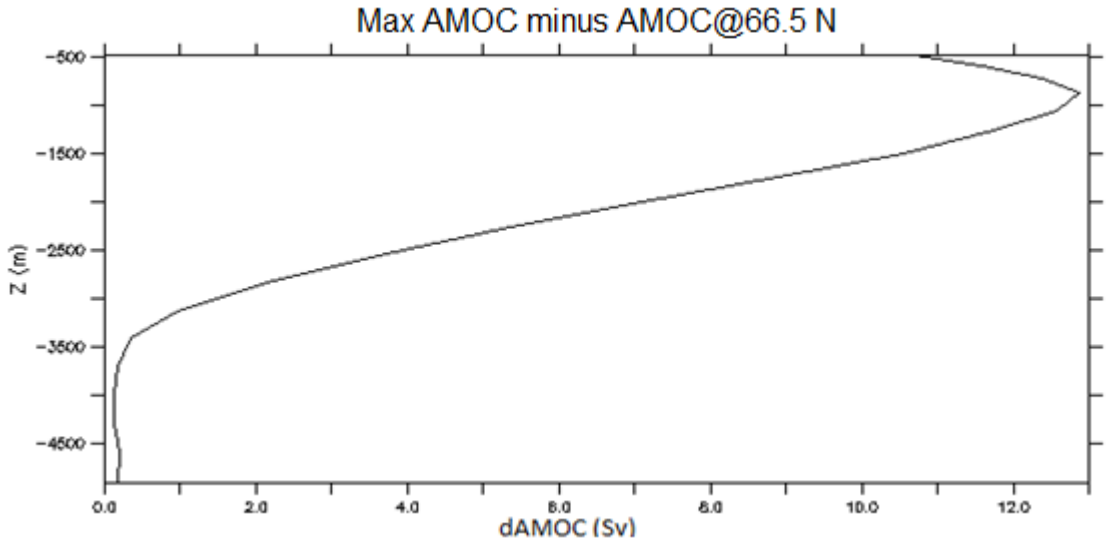

Figure 18 - Horizontal AMOC gradient of the average of 2030 – 2049 in the control run CTRL

Table 4 - Values of horizontal AMOC gradient

Model run:	Depth of max dAMOC (m)	dAMOC (Max AMOC – AMOC@66.5N (Sv)
P050>70	-880.5	14.13
P100>70	-880.5	12.87
P150>70	-880.5	11.94
P200>70	-880.5	11.26
P400>70	-880.5	9.64
P400>80	-880.5	12.16

4.4.1 Sinking in the control run

4.4.1.1 Overflows GS ridge

Figure 20 shows the time averaged vertical velocity (sinking) at a depth of 880.5 m for run CTRL. The largest vertical velocities are around the Greenland Scotland Ridge (GS Ridge). The up- and downwelling around the ridge are the results of three major overflows at Denmark Strait, the Iceland Faroe Ridge and through the Faroe Bank Channel, where the water flows from the Nordic Seas into the North Atlantic Ocean. Table 5 shows the vertical mass transport for these up- and downwelling regions in the red boxes in Figure 20. The table shows that there is much more downwelling than upwelling. The water in the Nordic Seas at the overflow depth (which is shallower than 880 m) has a higher density than the water in the North Atlantic Ocean at the same depth, as shown in Figure 19

for a depth of 800m. Because of the density differences, overflows from the Nordic Seas to the North Atlantic Ocean occur. Since this part of the overflow is originating from a depth above 880 m (the depth at which the up- and downwelling is calculated) this is not part of the upwelling which crosses 880 m of depth. However, when this flow enters the North Atlantic Ocean, the water will have a relatively high density and will indeed sink and cross the level of 880 m. Also entrainment can cause a difference between the up- and downwelling.

Observations of overflow over the Greenland Scotland ridge are different from the vertical mass transports in run CTRL as shown in Table 5. The total is difference between the downwelling and the observations of overflow is 0.86 Sv.

Table 5 - Up- and downwelling along the Greenland Scotland Ridge

Region	**Vertical mass transport in run CTRL**	**Observations of GS-ridge overflow** (Olsen, Hansen, Quadfasel, & Østerhus, 2008)
Denmark Strait upwelling	0.76 Sv	3 Sv
Denmark Strait downwelling	-1.39 Sv	
Iceland Faroe Ridge downwelling	-1.65 Sv	1 Sv
Faroe Bank Channel upwelling	1.33 Sv	2.1 Sv
Faroe Bank Channel downwelling	-2.20 Sv	
Total upwelling GSridge	**2.09 Sv**	**6.1 Sv**
Total downwelling GSridge	**-5.24 Sv**	

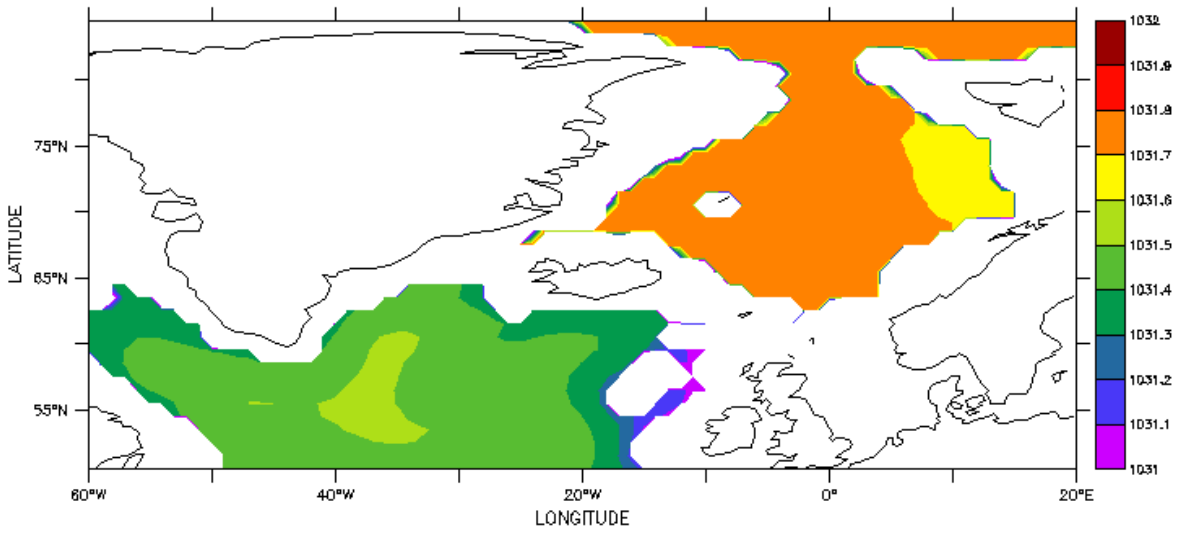

Figure 19 – Densities in the Nordic Seas and North Atlantic Ocean at a depth of 800 m

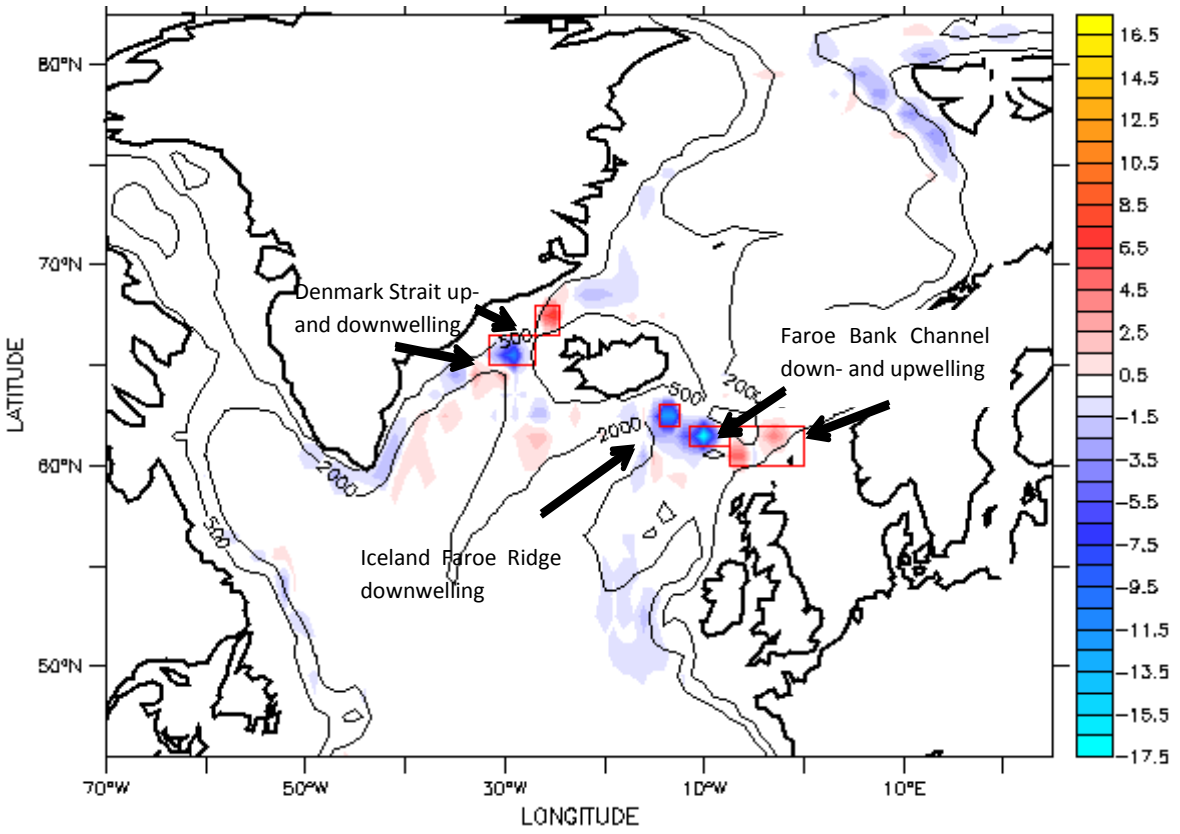

Figure 20 – Vertical velocity at 880 m averaged over the last 20 years of the model runs in m/day for run CTRL, up- and downwelling areas as a result of GS ridge overflow are shown in the red squares

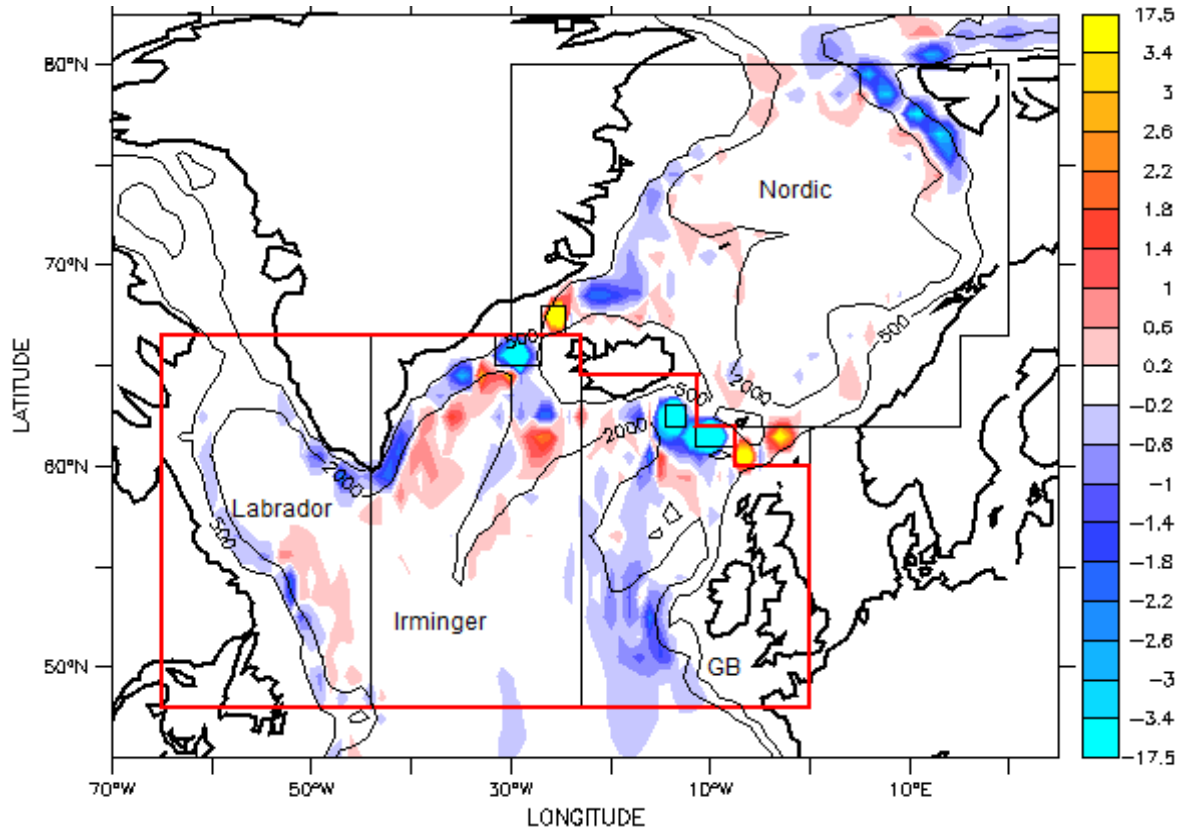

Figure 21 – Same as Figure 20 but with a different scale emphasizing other sinking locations than the overflow locations

4.4.1.2 *Atlantic overturning*

Figure 21 shows the same vertical velocities as Figure 20, but on a different color scale such that the other regions with smaller vertical velocities also become visible. In this figure the North Atlantic Ocean is divided into four regions, the Nordic, Labrador, Irminger and GB region.

Shown in Figure 21 is that in the Labrador, Irminger and Nordic regions, most of the sinking occurs near the continental boundary as expected following Spall & Pickart (2001). In the GB region, a large amount of sinking occurs in an unexpected location. Figure 22 shows the bottom topography and the horizontal flow at a depth of 880 meters of this region. If Figure 21 and Figure 22 are compared, it turns out that the sinking corresponds with large gradients in topography and a place where an eastern flow meets a western flow (15°W, 51°N). Possibly this creates a lot of friction which facilitates the downwelling.

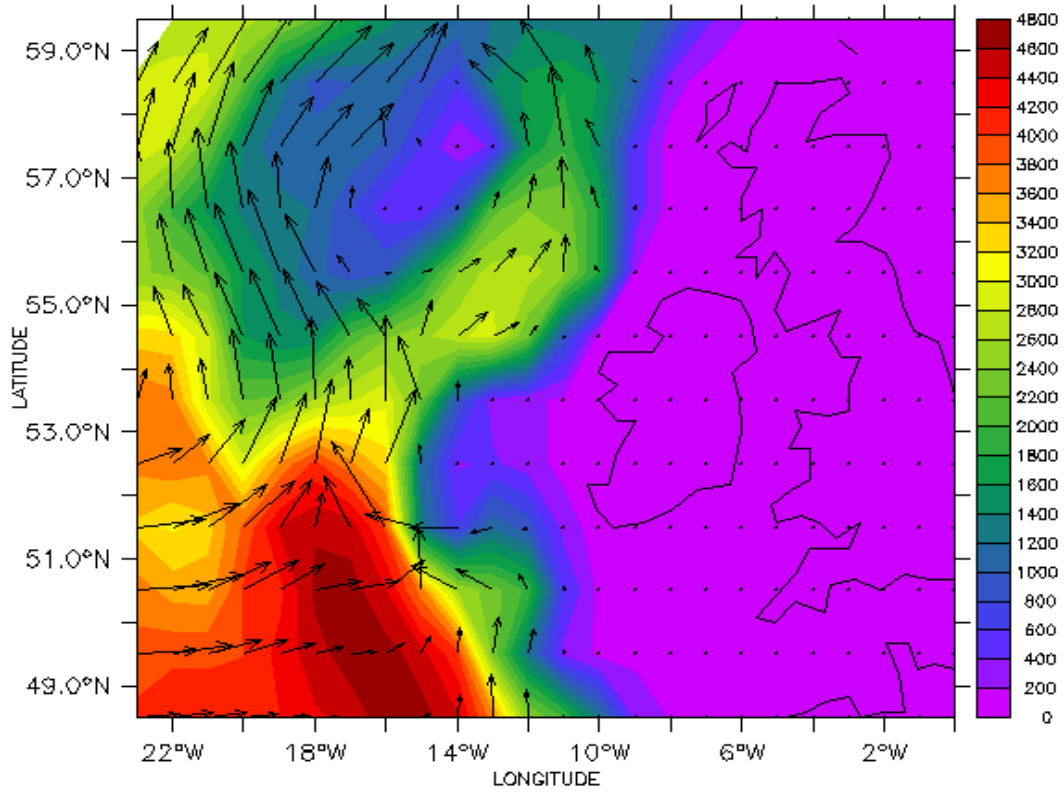

Figure 22 - Depth (color scale) and Flow velocities (arrows) in the GB region

Besides the sinking regions in Figure 21, there are two other main sinking regions. These are a sinking region in the Arctic and a sinking region as a result of the convection occuring in the Mediterranean Sea as shown in Figure 31.

According to the general theory, the main part of the AMOC is formed in the North Atlantic Ocean and a small part in the Mediterranean Sea (Marshall & Schott, 1999). Therefore the total amount of sinking occurring in these regions is expected to approximate the strength of the AMOC. However, since there is an exchange of waters with the Arctic, the dAMOC value of 12.91 Sv calculated in section 4.4 should be approximated. To check whether this is correct the vertical mass transports in the Labrador, Irminger and GB region including the overflows of the GS ridge and Mediterranean are summed up in Table 6. The total sinking occurring in the North Atlantic turns out to be 10.93 Sv. This

value approximates the 12.91 Sv of the dAMOC. The difference can be explained because it is also possible that sinking occurs outside of the regions in Figure 21, for example south of the Irminger and GB regions. Another cause can be that the boundary between the North Atlantic and the Arctic Ocean is picked to be at 66.5 °N while the boundary is in fact the Greenland Scotland ridge. The zonal integration in the calculation of the AMOC makes that the flows in the southern part of the Nordic Seas are also taken into account in the AMOC at 66.5 °N.

Table 6 - Vertical mass transport in run CTRL

Region	Vertical mass transport in run CTRL
Labrador	-1.00 Sv
Irminger	+0.47 Sv
GB	-4.92 Sv
GS downwelling	-5.24 Sv
Mediterranean	-0.23 Sv
Total	**-10.93 Sv**

4.4.1.3 Arctic overturning

The overturning circulation in the Arctic Ocean has a value of roughly 4 Sv in run CTRL according to Figure 17. The sum of the vertical mass transport in the Arctic, Nordic and upwelling regions at the GS Ridge should approximate this value. To check whether this is the case the total sinking in the Arctic Ocean and the Nordic Seas (including upwelling at the GS Ridge) is calculated in Table 7 and the total value is -3.78 Sv. This makes that the amount of sinking in the Arctic Ocean is indeed approximately the same as the same as the overturning strength in the Arctic Ocean.

Table 7 - Vertical mass transport in run CTRL

Region	Vertical mass transport in run CTRL
Arctic	-5.25 Sv
Nordic	-0.62 Sv
GS upwelling	+2.09 Sv
Total	**-3.78 Sv**

4.4.2 Changes in sinking due to changes in precipitation

Figure 23 shows the change in vertical velocity for run P400>70 compared to run CTRL. The largest changes in vertical velocity appear to be at the overflows at the Greenland Scotland Ridge. The downwelling as a result of the overflows decreases up to 8.5 m/day. The upwelling at the overflows decreases up to 7.5 m/day at Denmark Strait and with values up to 3.5 m/day at the Faroe Bank Channel. Figure 23 also shows a large decline in vertical velocity near the southwest boundary of Spitsbergen, the sinking values decrease to 3.5 m/day. In Figure 24 similar declines in vertical velocity can be seen in the Labrador Sea. The locations of these decreases in vertical flow velocity correspond with the decrease of the mixed layer depth in Figure 14. The decrease in mixed layer depth indicates less convection. If there is less convection, less heat will be transported towards the interior of the convection region and the density differences in the boundary current become smaller, according to Equation 9 this does indeed make less sinking occur. Near the coast of Norway the opposite is happening, the mixed layer depth moves to this location and the sinking increases.

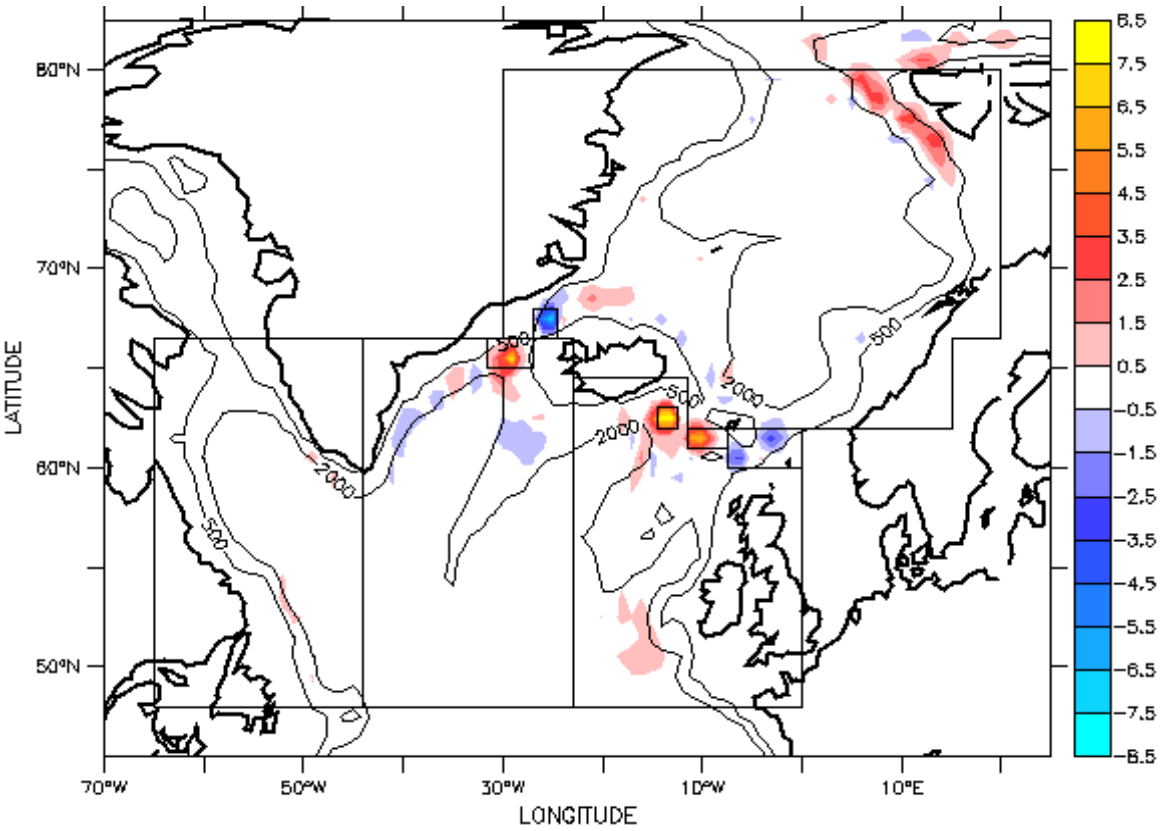

Figure 23 - Change in vertical velocities averaged over the last 20 years of the run P400>70 vs run CTRL in m/day

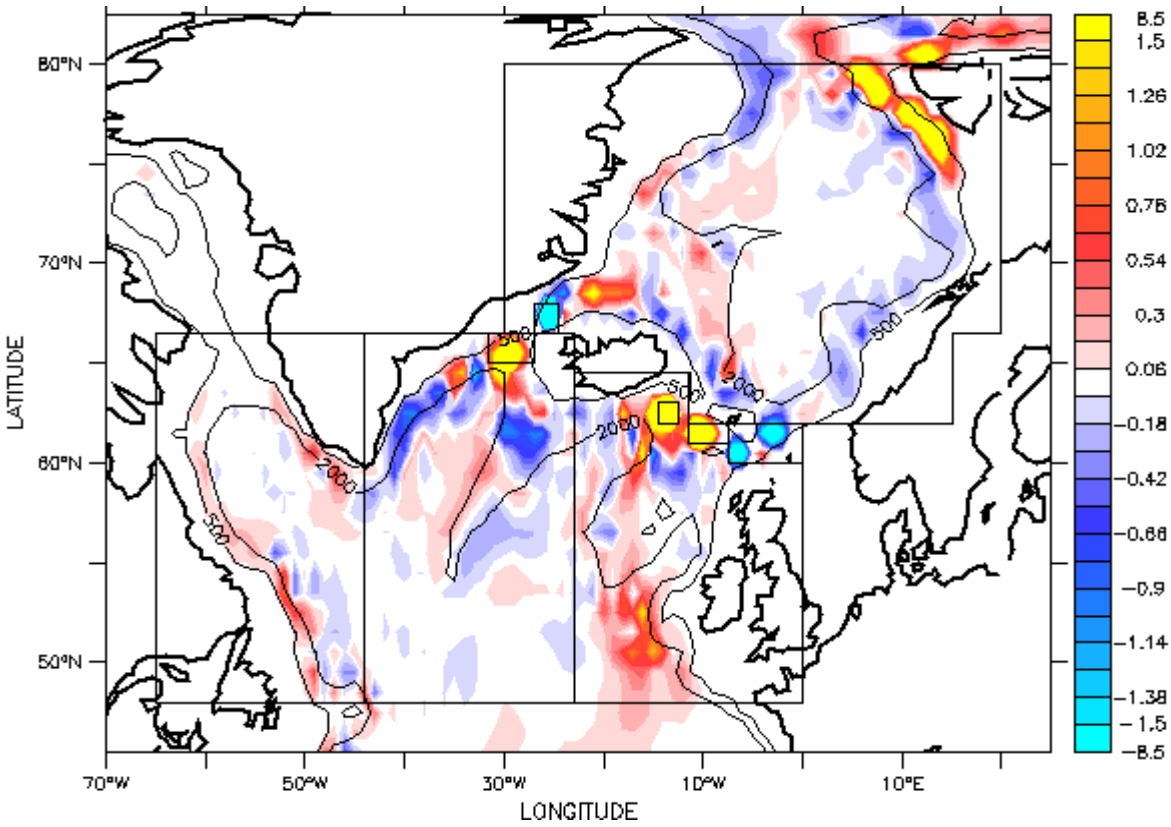

Figure 24 - Same as Figure 23 but with a different scale emphasizing other sinking locations than the overflow locations

Figure 25 shows the up- and downwelling at the GS ridge. In all model runs there is a decreasing trend. All three downwelling regions show a similar decline in the amount of downwelling. The model run P400>80 shows that if the precipitation is located above 80 °N the overflows have a smaller change compared to the precipitation above 70 °N.

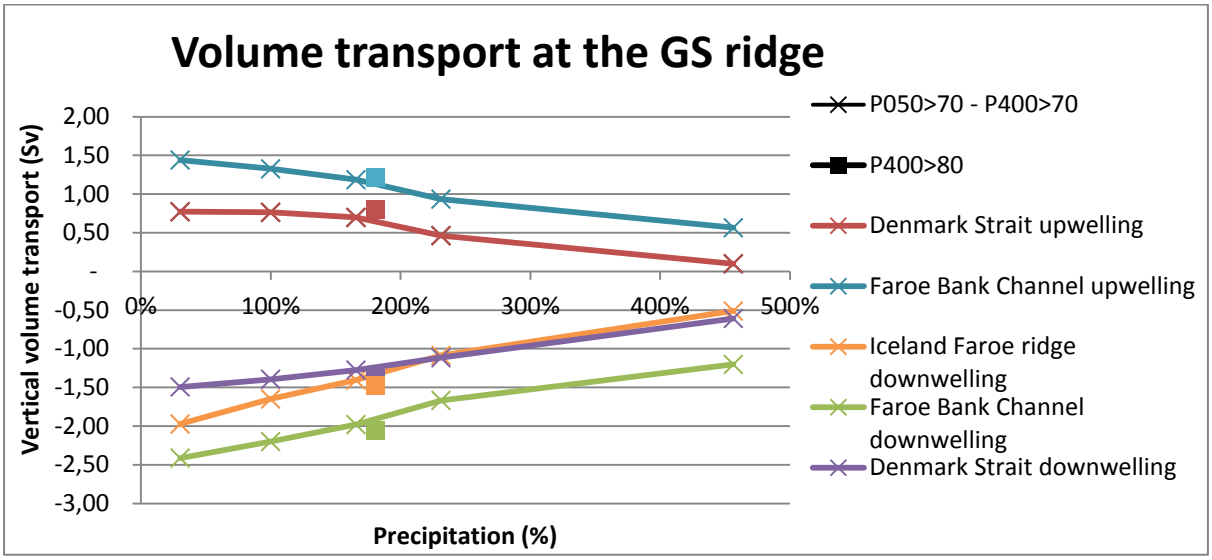

Figure 25 -Vertical volume transport (Sv) at the GS Ridge at 880 m of depth

According to Whitehead (1998) the changes in overflow are due to a smaller density difference upstream of the sills and downstream of the sills. Table 8 shows the densities upstream and downstream of Denmark Strait, the Iceland Faroe Ridge and the Faroe Bank Channel. It is assumed that the largest densities occur at the depth of the sill. Although the change in density up- and downstream of the sill gets lower, the decrease in $\Delta\sigma_t$ does not directly correspond to the change in vertical volume transport if the $\Delta\sigma_t$ in Table 8 are compared to the vertical volume transports in Figure 25.

Table 8 - Densities up- and downstream of the sills for run CTRL and run P400>70

	Depth sill	**CTRL**			**P400>70**		
		σ_t Up	σ_t Down	$\Delta\boldsymbol{\sigma_t}$	σ_t Up	σ_t Down	$\Delta\boldsymbol{\sigma_t}$
Denmark Strait	550	30.54	30.15	**0.28**	30.21	30.10	**0.11**
Iceland Faroe Ridge	600	31.11	30.54	**0.57**	30.93	30.42	**0.51**
Faroe Bank Channel	750	31.77	31.41	**0.36**	30.67	31.31	**0.35**

Figure 26 shows the mass transport (Sv) for the different regions for the different runs. The regions with the largest change in sinking with increase in precipitation are the GB region and the downwelling in the GS-ridge. All but the sinking in the Irminger region show a declining trend in mass transport as the amount of precipitation increases. The increase in the amount of sinking in the Irminger region corresponds with the relatively large mixed layer depths in this region in run P400>70 (shown in Figure 14).

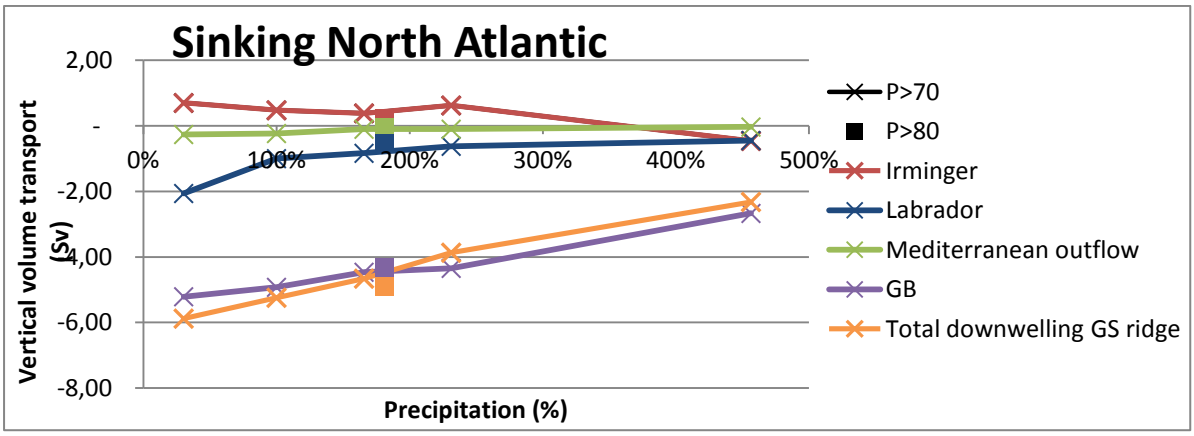

Figure 26 –Sinking (Sv) in the North Atlantic Ocean (and Mediterranean outflow)

Figure 27 shows the change of sinking between run P400>70 and run CTRL in blue and between NPE946>80 and NCTRL in purple for the different regions in the North Atlantic Ocean. From this figure it becomes clear that the largest part of the decline in AMOC in run P400>70 comes from the GB region and from the overflow over the Greenland Scotland ridge. This is probably because the sinking in these regions is also in the control runs much larger than the sinking in the other regions and therefore the largest part of change also comes from these regions. In the model run NPE946>80 the sinking in the Labrador Sea is also responsible for a large part of the decline of the AMOC. This corresponds with the complete collapse of the mixed layer depth in this region in run NPE946>80 (shown in figure Figure 14). The downwelling as a result of GS overflow is much less affected in the >80 model runs compared to the >70 model run, this corresponds with the small change in convection in the Nordic Sea.

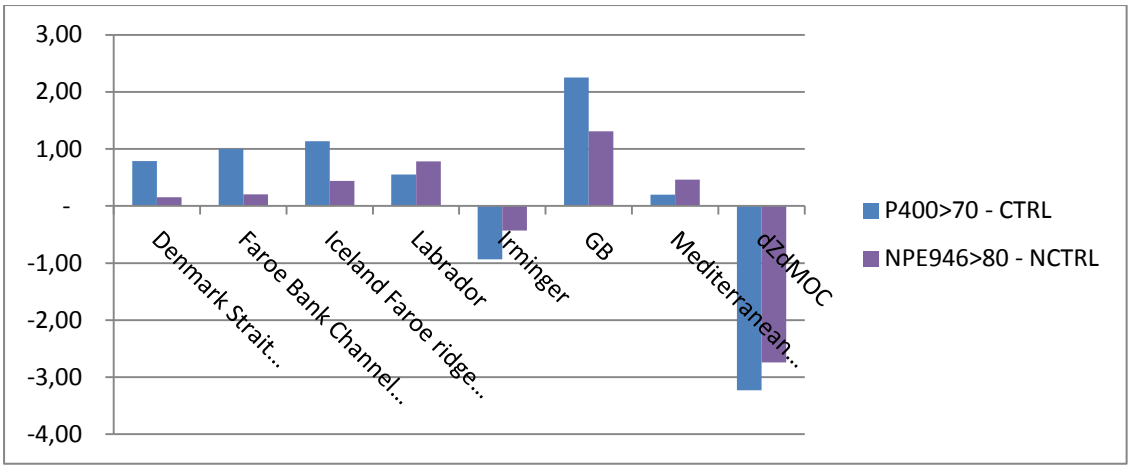

Figure 27 – Change of sinking (Sv) in the North Atlantic Ocean (and Mediterranean outflow) and change in dZdMOC (Sv)

Figure 28 shows the dAMOC and the sinking in the Labrador, Irminger, GB, GS downwelling and Mediterranean regions. Both variables show a declining trend in both sets of runs, the runs performed by Bintanja & Selten (2014) (solid lines) and the new model runs (dotted lines). In the model runs performed by Bintanja & Selten, the lines are diverting, this indicates that with increasing precipitation the sinking occurs more in locations outside of the regions for which the sinking is calculated.

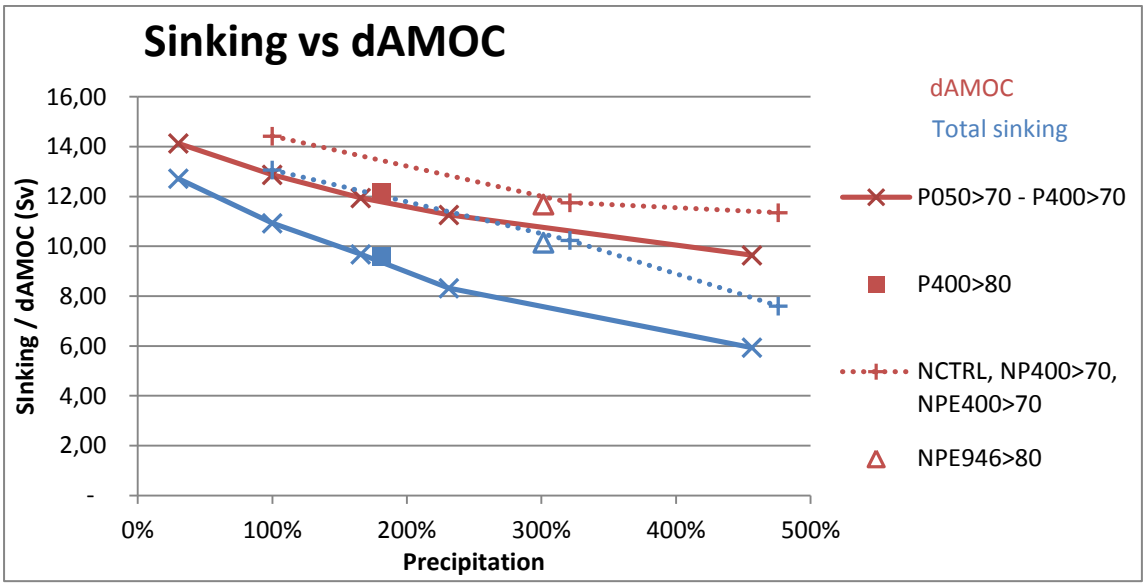

Figure 28 - dAMOC and total sinking (sinking in the Labrador, Irminger, GB, GS downwelling and the Mediterranean region)

5 Discussion

The first point of discussion in the report is that the extra precipitation in the model runs is artificially added to the system. While in a real world situation the increase in precipitation in the Arctic is a result of increased evaporation in the Arctic and Atlantic Ocean. This means that the way the water is added to the system in the model runs results in an Atlantic Ocean which has a surface layer which is too fresh (because there is no increased evaporation in the model runs). Since the surface waters of the Atlantic Ocean are transported towards the North Atlantic Ocean (where the sinking happens) the AMOC has a smaller strength in the model runs than it would have in a real world situation. So the effect of an increase in precipitation is overestimated because of this.

In this study it is chosen to work with the 1 degree resolution in the EC-Earth model. This choice is made because of computational reasons. The relatively course grid size results in a bathymetry which is not completely accurate. Especially near the Greenland Scotland ridge this is an important factor. If the passages in the Greenland Scotland Ridge are overestimated in size, this can result in too much exchange of waters between the North Atlantic Ocean and the Arctic Ocean. At the other side, too small passages can result in underestimations of the amount of exchange.

As mentioned in part 3.2.2 the model does not simulate all variables in accordance to observations, the possible effects on this study is also mentioned in part 3.2.2. While reading the conclusions, it has to be taken in mind that this research is done with only one model. The results do therefore only show a possible reaction of the system. The most important variable in the model which is not modeled in line with observations is the AMOC. In EC-Earth the AMOC has a strength which is relatively low to the observations (+-14 Sv in the model, +-18 Sv in observations). This results in an underestimation of the sensitivity of the AMOC strength.

In this study the precipitation is only increased above the water and sea ice in the Arctic Ocean, not above the land. This will probably not have a large influence on the model results because precipitation in the Arctic will most likely be snow and change into land ice. This means that it takes a long time for this precipitation to arrive in the ocean because the land ice first has to melt before it will run off into the ocean.

In this study a larger increase in precipitation above the Arctic Ocean has been simulated compared to the expectations. In many situations the most extreme model run P400>70 is used. The precipitation in this model run is 456 % of the precipitation in the control run, while the projected increase in precipitation is only 50 %. This makes that many changes shown in this report are strongly exaggerated. This is done to make the processes behind the changes more clear. The sensitivity analysis also shows the values of the changes for the other model runs including the run in which the precipitation is close to the projected increase in precipitation (166 % of the precipitation in the control run).

Most of the variables that the model simulated did not reach the equilibrium state (when there is no more trend visible) in the 40 years of simulation. This is shown in Figure 29 for a model run which had a simulation period of 100 years. From this figure it becomes clear that the AMOC is in equilibrium around the year 2100. For the results in this report this means that the value gives for the different variables (SSS, MLD, AMOC etc.) are not yet the final values. It is expected that when the model runs longer, the variables show stronger signals. However, to find and study the processes

that lead to a change in AMOC strength it does not matter whether the equilibrium state has been reached or not.

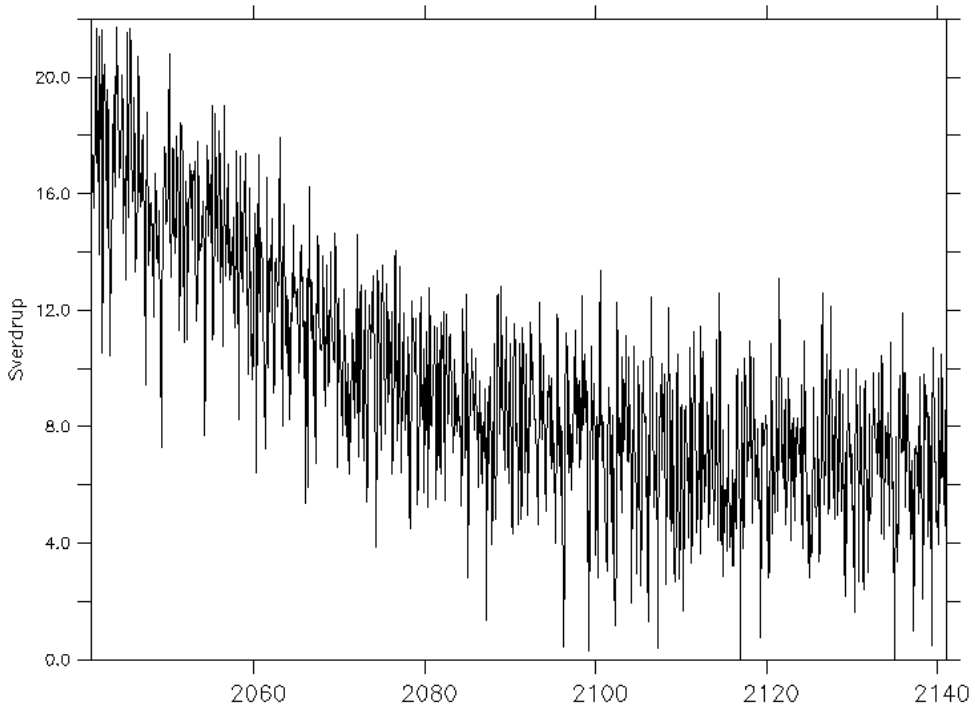

Figure 29 - AMOC strength (Sv) 100 year model run

6 Conclusions and recommendations

6.1 Conclusions

How sensitive is the strength of the AMOC to the intensity of precipitation in the Arctic region?

In this study the effect of an increase in precipitation above the Arctic has been analyzed. In the sensitivity analysis it turned out that the sea surface salinities in Fram Strait and Davis Strait change up to 6.8 % in the model run in which the precipitation was increased to 400 % of the original precipitation above 70 degrees north. Compared to the natural variability this is a large change. Absolutely seen, the mixed layer depths are much more sensitive to an increase in precipitation above the Arctic Ocean, however, compared to the natural variability the changes are comparable to the changes in sea surface salinity. The maximum values of the mixed layer depth in the Nordic Seas and Labrador Sea decline as much as 76 %. Also the AMOC is also much more sensitive than the sea surface salinities, but less sensitive than the mixed layer depth. In run P400>70 the decrease in AMOC strength is 43 %.

How does the sea surface salinity anomaly propagate towards the convection regions?

The sea surface salinity anomaly travels from Fram Strait towards Denmark Strait, however, the relatively fresh water does not reach the convection region in the Nordic Seas directly. This is because of the existing gyre in the Nordic Seas which makes that the surface waters come from the south and travels counterclockwise, pushing the East Greenland Current against the coast of Greenland. After Denmark Strait the relatively freshwater is mixed with North Atlantic water which decreases the anomaly before reaching the Labrador Sea.

How does the change in convection as a result of an increase in precipitation in the Arctic affect the strength of the Atlantic meridional overturning circulation?

The mixed layer depth, which is an indicator for the amount of convection, in the Nordic Seas and the Labrador/ Irminger Seas is strongly affected by a change in precipitation. The density profiles show that a layer of relatively fresh water will indeed form on top of the denser waters below. This makes the convection occurring in these regions much less. In the Labrador and Irminger seas this does not affect the AMOC directly. In the Nordic Seas however, less convection means that the deeper waters in the Nordic Seas are not as dense as without the increase in precipitation. This causes that the density differences between the Nordic Seas and the North Atlantic Ocean to decrease. This decrease in density difference makes that there is less deep water flowing over the Greenland Scotland Ridge and that there is less cascading water forming the initial branch of the AMOC.

What is the relationship between sinking in the North Atlantic Ocean and the strength of the AMOC?

The sinking in the North Atlantic Ocean is responsible for a large part of the strength of the AMOC. In the control run 10.93 Sv of the 12.91 Sv of the strength of the AMOC originates in the North Atlantic Ocean. The most important sinking regions are the GB region and the sinking as a result of the Greenland Scotland ridge overflow. If the precipitation is increased most of the regions with sinking show a decrease in the amount of sinking. This is as expected as the net sinking is also depending of the mixed layer depth. With an increase in precipitation above the Arctic Ocean, there is a larger

part of the AMOC formed outside of the North Atlantic region since the sinking in this region decreases to 5.94 Sv of the 9.64 Sv of the AMOC.

How does the AMOC respond to a more centered increase in precipitation in the Arctic region above 80 °N?

If the increase in precipitation is only located north of 80 °N instead of 70 °N, the processes respond differently, the average value of the mixed layer in the Nordic Seas is affected less. Also the sinking in the North Atlantic Ocean decreased less. The processes respond differently because the precipitation is not directly increased above the Nordic Seas, the relatively fresh water has to travel from further so it will get mixed with less fresh surface waters on the way. In the AMOC this effect is no longer visible and the AMOC decreases as much as would have been the case if the precipitation increased in the region above 70 °N.

6.2 Recommendations for further research

Since the bathymetry is important near small passages like those at the Greenland Scotland Ridge, it is recommended to study the sinking in the North Atlantic Ocean with a smaller grid size. A smaller grid size will better estimate the real bathymetry and the values of the parameters will be more accurate to their real location.

The sinking in the GB region is not in line with observations. In this study it is assumed to be because of too much friction in that region. It is recommended that this location is studied in more detail so that the cause of the sinking in this region becomes clearer.

The Arctic Ocean is not a known location for sinking to occur. In the EC-Earth version 2.3 used in this study the model does show a large amount of sinking in this region. It is recommended to find out what causes the sinking in the Arctic to happen. It could either be a flaw in the model, but there is also a possibility that there is actually sinking happening in the Arctic Ocean. To verify this, the sinking in the Arctic region should be studied in other model as well to see if they show the same behavior. If this is the case, it could be that there is actually sinking in the Arctic, measurements can give the answer to this question.

As the precipitation increases, a larger part of the AMOC is formed outside of the North Atlantic Ocean. In this study it is not analyzed where this exactly is. To fully understand the system it is recommended to do more research to this phenomenon.

Bibliography

Androsov, A., Rubino, A., Romeiser, R., & Sein, D. V. (2005). Open-ocean convection in the Greenland Sea: preconditioning through a mesoscale chimney and detectability in SAR imagery studied with a hierarchy of nested numerical models. *Meteorologische Zeitschrift, 14*(6), 693-702. doi:10.1127/0941-2948/2005/0078

Bengtsson, L., Hodges, K. I., Koumoutsaris, S., Zahn, M., & Keenlyside, N. (2011). The changing atmospheric water cycle in Polar Regions in a warmer climate. *Tellus A, 63*(5), 907-920. doi:10.111/j.1600-0870.2011.00534.x

Bintanja, R., & Selten, F. (2014). Future increases in Arctic precipitation linked to local evaporation and sea-ice retreat. *Nature, 509*, 479-482. doi:10.1038/nature13259

Bintanja, R., Oldenborgh, G., Drijfhout, S. S., Wouters, B., & Katsman, C. (2013). Important role for ocean warming and increased ice-shelf melt in Antarctic sea-ice expansion. *Nature Geoscience, 6*, 376-379. doi:10.1038/NGEO1767

Bouillon, S., Maqueda, M. Á., Legat, V., & Fichefet, T. (2009). An elastic-viscous-plastic sea ice model formulated on Arakawa B and C grids. *Ocean Modelling, 27*(3-4), 174-184. doi:10.1016/j.ocemod.2009.01.004

Brown, J., Colling, A., Park, D., Phillips, J., Rothery, D., & Wright, J. (1989). *Ocean cirulation* (1 ed.). (G. Bearman, Red.) The Open University.

Collins, M., Knutti, R., Arblaster, J., Dufresne, J.-L., Fichefet, T., Friedlingstein, P., . . . Wehner, M. (2013). Long-term Climate Change: Projections, Commitments and Irreversibility. In T. Stocker, D. Qin, G.-K. Plattner, M. Tignor, S. Allen, J. Boschung, . . . P. Midgley, *Climate Change 2013: The Physical Science Basis. Contribution of Working Group I to the Fifth Assessment Report of the Intergovernmental Panel on Climate Change.* Cambridge, United Kingdom and New York, NY, USA: Cambridge University Press.

Curry, R. (2012). *Atlantic Meridional Overturning Circulation*. Opgeroepen op 08 17, 2015, van The Encyclopedia of the Earth: http://www.eoearth.org/view/article/150290

Davis, J. C. (2002). *Statistics and data analysis in geology.* John Wiley & Sons.

Dixon, K. W., Delworth, T. L., Spelman, M. J., & Stouffer, R. J. (1999). The influence of transient surface fluxes on North Atlantic overturning in a coupled GCM climate changes experiment. *Geophysical Research Letters, 26*(17), pp. 2749-2752. doi:10.1029/1999GL900571

Drijfhout, S. S., Marshall, D. P., & Dijkstra, H. A. (2013). Chapter 11 - Conceptual Models of the Wind-Driven and Thermohaline Circulation. In G. Siedler, S. M. Griffies, J. Gould, & J. A. Church (Red.), *Ocean circulation & climate* (2 ed., Vol. 103, pp. 257-282). Elsevier.

Fischer, N., & Jungclaus, J. (2010). Effects of orbital forcing on atmosphere and ocean heat transports in Holocene and Eemian climate simulations with a comprehensive Earth system model. *Climate of the Past, 6*, pp. 155-168. doi:10.5194/cp-6-155-2010

Grieco, G., & Masina, S. (2009). *Implementation of NEMO-OPA in configuration ORCA-R025.* Centro Euro-Mediterraneo per i Cambiamenti Climatici.

Hazeleger, W., & Bintanja, R. (2014). Accomplishments, Current Status and Future Plans of EC-Earth: a European Earth System Model.

Iovino, D., Straneo, F., & Spall, M. A. (2008). On the effect of a sill on dense water formation in a marginal sea. *Journal of Marine Research, 66*, 325-345. doi:10.1357/002224008786176016

Kanzow, T., Cunningham, S., Johns, W., Hirschi, J. J.-M., Marotzke, J., Baringer, M., . . . Collins, J. (2010). Seasonal Variability of the Atlantic Meridional Overturning Circulation at 26.5°N. *Journal of Climate, 23*(21), 5678-5698. doi:10.1175/2010JCLI3389.1

Katsman, C. A., Spall, M. A., & Pickart, R. S. (2004). Boundary current eddies and their role in the restratification of the Labrador Sea. *Journal of Physical Oceanography, 34*(9), 1967-1983. doi:10.1175/1520-0485(2004)034<1967:BCEATR>2.0.CO;2

Koenigk, T., Brodeau, L., Graversen, R. G., Karlsson, J., Svensson, G., Tjernström, M., . . . Wyser, K. (2012). Arctic climate change in 21st century CMIP5 simulations with EC-Earth. *40*(11-12), pp. 2719-2743. doi:10.1007/s00382-012-1505-y

La Forge du LEGI. (2015). *CDFTOOLS : A fortran package for diagnostics of ocean model output*. Opgeroepen op 08 3, 2015, van La Forge du LEGI: http://servforge.legi.grenoble-inp.fr/projects/CDFTOOLS

Lilly, J. M., Rhines, P. B., Visbeck, M., Davis, R., Lazier, J. R., Schott, F., & Farmer, D. (1999). Observing deep convection in the Labrador Sea during winter 1994/1995. *Journal of Physical Oceanography, 29*(8), 2065-2098. doi:10.1175/1520-0485(1999)029<2065:ODCITL>2.0.CO;2

Marshall, J., & Schott, F. (1999). Open-Ocean Convection: Observations, Theory, and Models. *Review of Geophysics, 37*(1), pp. 1-64. doi:10.1029/98RG02739

Masson-Delmotte, V., Schulz, M., Abe-Ouchi, A., Beer, J., Ganopolski, A., González Rouco, J., . . . Timmermann, A. (2013). Information from Paleoclimate archives. In T. Stocker, D. Qin, G.-K. Plattner, M. Tignor, S. Allen, J. Boschung, . . . P. Midgley, *Climate 2013: The Physical Science Basis. Contribution of working group I to the Fifth Assessment Report of the Intergovernmental panel on Climate Change.* Cambridge University Press, Cambridge, United Kingdom and New York, NY, USA.

Molines, J., & Treguier, A. (2006). *cdfmoc.f90*. Opgeroepen op 07 31, 2015, van La Forge du LEGI: http://servforge.legi.grenoble-inp.fr/projects/CDFTOOLS/browser/CDFTOOLS/trunk/cdfmoc.f90?rev=168

Molines, J., Dussin, R., & Balmaseda, M. (2011). *root / branches /CDFTOOLS_3_dev / cdftransport.f90*. Opgeroepen op 08 03, 2015, van La Forge du LEGI: http://servforge.legi.grenoble-inp.fr/projects/CDFTOOLS/browser/branches/CDFTOOLS_3_dev/cdftransport.f90

Olbers, D., Willebrand, J., & Eden, C. (2012). *Ocean Dynamics.* Springer. doi:10.1007/978-3-642-23450-7

Olsen, S. M., Hansen, B., Quadfasel, D., & Østerhus, S. (2008). Observed and modelled stability of overflow across the Greenland-Scotland ridge. *Nature, 455*, 519-523. doi:10.1038/nature07302

Paluszkiewicz, T., Denbo, D. W., & Garwood, R. W. (1994). Deep convection plumes in the ocean. *Oceanography, 7*(2). doi:10.5670/oceanog.1994.01

Robertson, R., Visbeck, M., Gordon, A. L., & Fahrbach, E. (2002). Long-term temperature trends in the deep waters of the Weddell Sea. *Deep-Sea Research II Topical studies in oceanography, 49*(21), 4791-4806. doi:10.1016/S0967-0645(02)00159-5

Spall, M. A., & Pickart, R. S. (2001). Where does dense water sink? A subpolar gyre example. *Journal of Physical Oceanography, 31*, 810-826. doi:10.1175/1520-0485(2001)031<0810:WDDWSA>2.0.CO;2

Sterl, A., Bintanja, R., Brodeau, L., Gleeson, E., Koenigk, T., Schmith, T., . . . Yang, S. (2012). A look at the ocean in the EC-Earth climate model. *Climate Dynamics, 39*, 2631-2657. doi:10.1007/s00382-011-1239-2

Tsimplis, M., & Bryden, H. (2000). Estimation of the transports through the Strait of Gibraltar. *Deep Sea Research Part I: Oceanographic Research Papers, 47*(12), 2219-2242. doi:10.1016/S0967-0637(00)00024-8

Vaughan, D., Comiso, J., Allison, I., Carrasco, J., Kwok, R., Mote, P., . . . Zhang, T. (2013). Observations: Cryosphere. In T. Stocker, D. Qin, G.-K. Plattner, M. Tignor, S. Allen, J. Boschung, . . . P. Midgley, *Climate 2013: The Physical Science Basis. Contribution of working group I to the Fifth Assessment Report of the Intergovernmental panel on Climate Change .* Cambridge University Press, Cambridge, United Kingdom and New York, NY, USA.

Whitehead, J. (1998). Topographic control of oceanic flows in deep passages and straits. *Reviews of geophysics, 36*(3), 423-440. doi:10.1029/98RG01014

Appendix

A. Sensitivity analysis

Table 9 - Sensitivity of the sea surface salinities in Davis, Denmark and Fram strait in kg/m^3 (averaged over the last 20 years of the model runs)

Run	ΔP_{net}	SSS Davis (kg/m^3)	Diff vs. CTRL (%)	STD (kg/m^3)	SSS Denmark (kg/m^3)	Diff vs. CTRL (%)	STD (kg/m^3)	SSS Fram (kg/m^3)	Diff vs. CTRL (%)	STD (kg/m^3)
P050>70	30 %	32,98	1.5	0,90	32,98	0.3	1,43	33,26	0.9	0,50
CTRL	100 %	32,50	0.0	1,00	32,89	0.0	0,83	32,96	0.0	0,51
P150>70	166 %	32,15	-1.1	0,91	32,79	-0.3	0,73	32,84	-0.4	0,52
P200>70	231 %	31,79	-2.2	1,19	32,65	-0.7	0,65	32,48	-1.5	0,48
P400>70	456 %	30,34	-6.7	0,69	31,72	-3.5	0,74	30,71	-6.8	0,66
P400>80	181 %	32,04	-1.4	1,05	32,67	-0.7	0,71	32,43	-1.6	0,56

Table 10 - Sensitivity of the sea surface salinities in Davis, Denmark and Fram strait in kg/m^3 (averaged over the last 20 years of the model runs)

Run	ΔP_{net}	SSS Davis (kg/m^3)	Diff vs. CTRL (%)	STD (kg/m^3)	SSS Denmark (kg/m^3)	Diff vs. CTRL (%)	STD (kg/m^3)	SSS Fram (kg/m^3)	Diff vs. CTRL (%)	STD (kg/m^3)
NCTRL	100 %	32.5	0.0	1.07	32.9	0.0	0.81	32.9	0.0	0.57
NPE400>70	321 %	30.1	-7.3	2.40	31.4	-4.4	0.64	31.0	-5.7	0.63
NP400>70	476 %	30.1	-7.4	0.76	31.6	-3.9	0.82	30.3	-7.8	0.76
NPE946>80	302 %	30.6	-5.8	1.16	31.1	-5.4	0.70	30.0	-8.7	0.74

Table 11 - Sensitivity of the area averaged MLDs in the Nordic and Labrador Seas (DJFMA averaged over the last 20 years of the model runs)

Run	ΔP_{net}	Ave MLD Nordic (m)	Diff vs. CTRL (%)	STD m)	Ave MLD Labrador (m)	Diff vs. CTRL (%)	STD (m)
P050>70	30 %	304	12.6	107	226	39.8	126
CTRL	100 %	270	0.0	77	161	0.0	72
P150>70	166 %	255	-5.7	79	142	-11.8	63
P200>70	231 %	230	-15.0	75	128	-20.6	59
P400>70	456 %	74	-72.8	32	61	-62.1	32
P400>80	181 %	246	-9.0	64	142	-11.8	72

Table 12 - Sensitivity of the area averaged MLDs in the Nordic and Labrador Seas (DJFMA averaged over the last 20 years of the model runs)

Run	ΔP_{net}	Ave MLD Nordic (m)	Diff vs. CTRL (%)	STD m)	Ave MLD Labrador (m)	Diff vs. CTRL (%)	STD (m)
NCTRL	100 %	237	0.0	97	184	0.0	81
NPE400>70	321 %	182	-22.9	52	113	-38.4	45
NP400>70	476 %	116	-51.0	47	100	-45.7	42
NPE946>80	302 %	198	-16.5	58	108	-41.1	44

Table 13 - Sensitivity of the maximum MLDs in the Nordic and Labrador Seas (DJFMA averaged over the last 20 years of the model runs)

Run	ΔP_{net}	Max MLD Nordic (m)	Diff vs. CTRL (%)	STD (m)	Max MLD Labrador (m)	Diff vs. CTRL (%)	STD (m)
P050>70	30 %	2071	82.5	989	945	49.5	398
CTRL	100 %	1135	0.0	266	631	0.0	203
P150>70	166 %	856	-24.6	193	560	-11.3	170
P200>70	231 %	691	-39.1	155	536	-15.1	212
P400>70	456 %	270	-76.2	84	362	-42.6	228
P400>80	181 %	867	-23.6	160	618	-2.0	282

Table 14 - Sensitivity of the maximum MLDs in the Nordic and Labrador Seas (DJFMA averaged over the last 20 years of the model runs)

Run	ΔP_{net}	Max MLD Nordic (m)	Diff vs. CTRL (%)	STD (m)	Max MLD Labrador (m)	Diff vs. CTRL (%)	STD (m)
NCTRL	100 %	1326	0.0	928	724	0.0	285
NPE400>70	321 %	644	-51.5	170	486	-32.9	222
NP400>70	476 %	355	-73.2	111	501	-30.9	229
NPE946>80	302 %	723	-45.5	163	477	-34.1	203

Table 15 - Sensitivity of the AMOC strength (averaged over last 20 years of the model runs)

Run	ΔP_{net}	AMOC (Sv)	Diff vs. CTRL (%)	STD (Sv)
P050>70	30 %	16.34	12.0	0.58
CTRL	100 %	14.59	0.0	0.40
P150>70	166 %	13.06	-10.5	0.61
P200>70	231 %	11.50	-21.2	0.68
P400>70	456 %	8.39	-42.5	1.62
P400>80	181 %	13.00	-10.9	0.74

Table 16 - Sensitivity of the AMOC strength (averaged over last 20 years of the model runs)

Run	ΔP_{net}	AMOC (Sv)	Diff vs. CTRL (%)	STD (Sv)
NCTRL	100 %	16.11	0.0	3.42
NPE400>70	321 %	12.61	-21.7	0.86
NP400>70	476 %	10.14	-37.0	0.96
NPE946>80	302 %	12.63	-21.6	0.77

B. Mixed layer depth

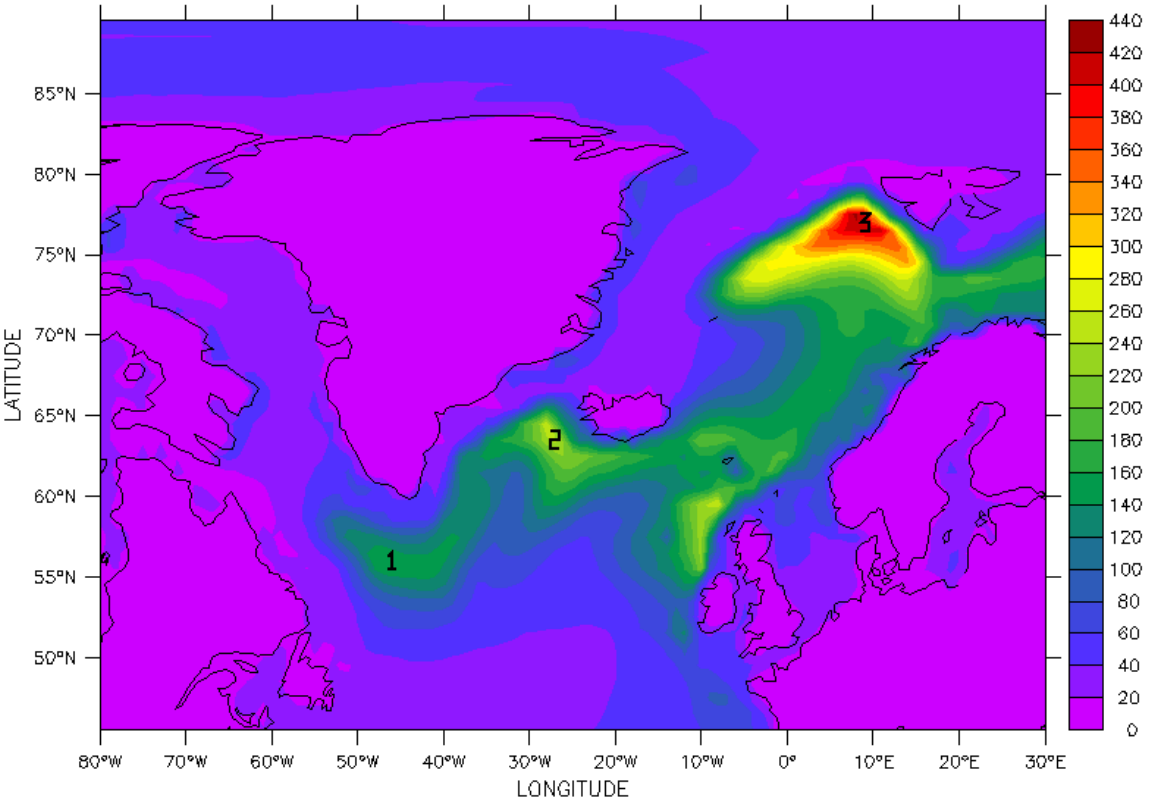

Figure 30 - Locations of density profiles MLD, 1 in the Labrador Sea, 2 in the Irminger Sea and 3 in the Nordic Seas

C. Sinking

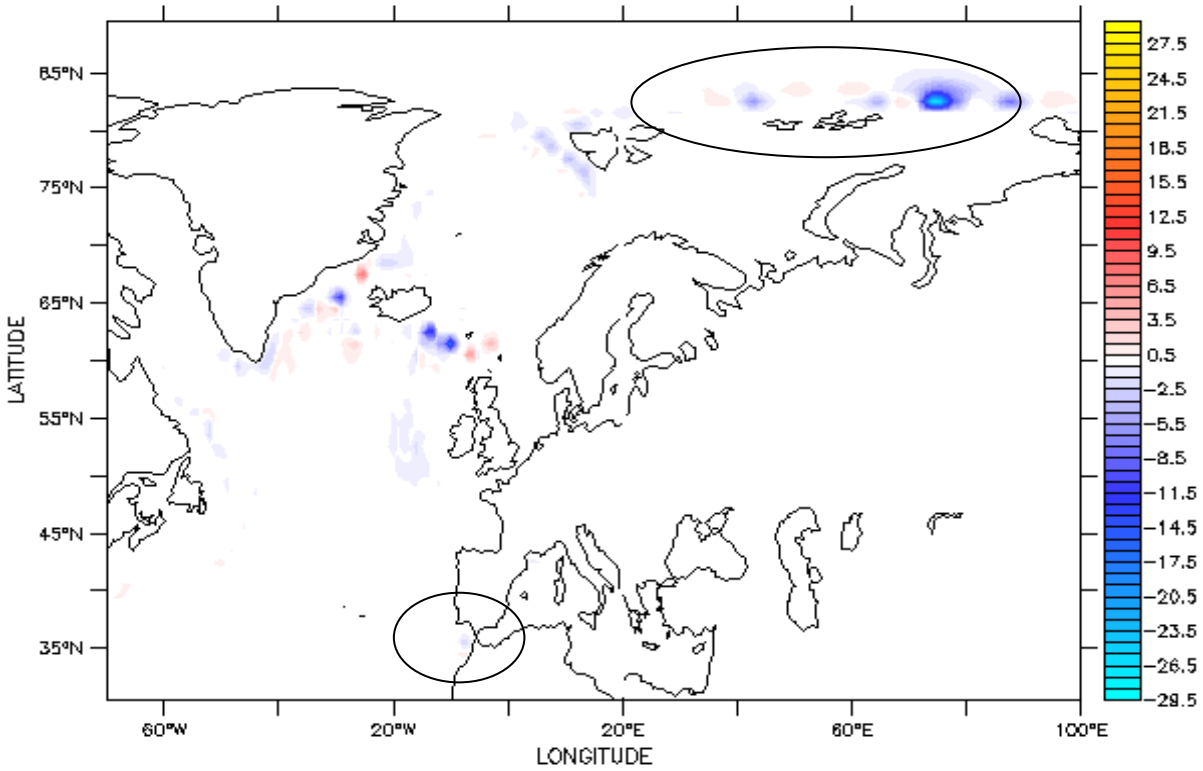

Figure 31 - Sinking (m/day) in the Arctic and sinking as a result of outflow of the Mediterranean

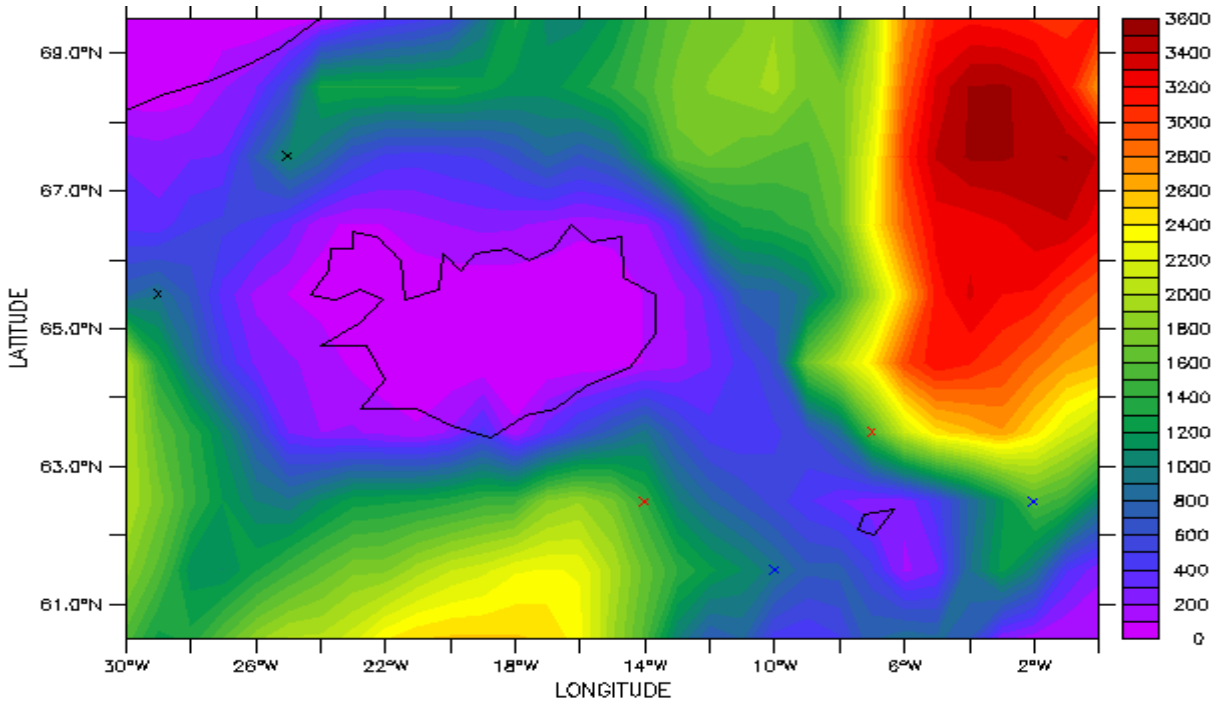

Figure 32 - Locations densities overflow